AJRCCM Articles in Press. Published on 19-July-2019 as 10.1164/rccm.201903-0639OC

Assessment of Inflammation in Pulmonary Artery Hypertension by ^{68}Ga-Mannosylated Human Serum Albumin

Jun-Bean Park[1,2], Minseok Suh[3], Ji Yong Park[3], Jin Kyun Park[4], Yong-il Kim[5], Hyunah Kim[1], Ye Seul Cho[1], Hyejeong Kang[1], Kibyung Kim[6], Jae-Hoon Choi[6], Jin-Wu Nam[6], Hyung-Kwan Kim[1,2], Yun-Sang Lee[3], Jae Min Jeong[3], Yong-Jin Kim[1,2], Jin Chul Paeng[3,7], and Seung-Pyo Lee[1,2,7]

[1]Cardiovascular Center, Seoul National University Hospital, Seoul, Republic of Korea,
[2]Division of Cardiology, Department of Internal Medicine, Seoul National University College of Medicine, Seoul, Korea, Seoul, Republic of Korea,
[3]Department of Nuclear Medicine, Seoul National University Hospital and Seoul National University College of Medicine, Seoul, Republic of Korea,
[4]Division of Rheumatology, Department of Internal Medicine, Seoul National University Hospital and Seoul National University College of Medicine, Seoul, Republic of Korea,
[5]Department of Nuclear Medicine, Asan Medical Center and University of Ulsan College of Medicine, Seoul, Republic of Korea,
[6]Department of Life Science, College of Natural Sciences, Hanyang University, Seoul, Republic of Korea
[7]These authors contributed equally as corresponding authors.

Total word count for the body of the manuscript: 3,801
Brief title: Molecular imaging with ^{68}Ga-NOTA-MSA PET for PAH
Subject Category: 9.35 Pulmonary Hypertension: Clinical-Diagnosis/Pathogenesis/Outcome

This article has an online data supplement, which is accessible from this issue's table of content online at www.atsjournals.org.

Author Contributions: J.B. Park, J.C. Paeng, and S.P. Lee contributed to the conception, design, analysis and interpretation of data. J.H. Choi, J.W. Nam, H.K. Kim, Y.S. Lee, J.M. Jeong, and Y.J. Kim contributed to the conception and design. M.Suh, J.Y Park, J.K. Park, Y.i. Kim, H. Kim, Y.S. Cho, H. Kang, and K. Nam contributed to the collection, analysis and interpretation of data. J.B. Park, J.C. Paeng, and S.P. Lee contributed to the drafting of and finalizing the manuscript. M. Suh, J.Y Park, J.K. Park, Y.i. Kim, H. Kim, Y.S. Cho, H. Kang, K. Nam, J.H. Choi, J.W. Nam, H.K. Kim, Y.S. Lee, J.M. Jeong, and Y.J. Kim contributed to revision of the manuscript by giving critical comments and important intellectual contents. All authors provided final approval of the manuscript submitted.

Sources of Funding: This research was supported by grants of the Korea Health Technology R&D Project through the Korea Health Industry Development Institute (KHIDI), funded by the Ministry of Health & Welfare, Republic of Korea (grant number: HI15C0399 and HI14C1277), and by the Global Frontier Project grant of National Research Foundation, funded by the Ministry of Science and ICT (MSIT), Republic of Korea (grant number: NRF-2017M3A6A4078907). There was no role of the study sponsors in the design and conduct of the study, in the collection, analysis, and interpretation of the data, and in the preparation, review, or approval of the manuscript.

Disclosures: None.

Address for correspondence:

Seung-Pyo Lee, MD, PhD
Cardiovascular Center, Seoul National University Hospital & Department of Internal Medicine, Seoul National University College of Medicine
101 Daehak-ro, Jongro-gu, Seoul, 03080, Korea
Tel: 82-2-2072-1980, FAX: 82-2-766-8904, E-mail: sproll1@snu.ac.kr

or

Jin Chul Paeng, MD, PhD
Department of Nuclear Medicine, Seoul National University Hospital & Seoul National University College of Medicine
101 Daehak-ro, Jongro-gu, Seoul, 03080, Korea
Tel: 82-2-2072-3341, FAX: 82-2-766-9083, E-mail: paengjc@snu.ac.kr

AJRCCM Articles in Press. Published on 19-July-2019 as 10.1164/rccm.201903-0639OC

ABSTRACT

Rationale: Diagnosis and monitoring of patients with pulmonary artery hypertension (PAH) is currently difficult.

Objectives: We aimed to develop a noninvasive imaging modality for PAH that tracks the infiltration of macrophages into the pulmonary vasculature, using a positron emission tomography (PET) agent, ^{68}Ga-2-(*p*-isothiocyanatobenzyl)-1,4,7-triazacyclononane-1,4,7-triacetic acid (NOTA) mannosylated human serum albumin (MSA), that targets the mannose receptor (MR).

Methods: We induced PAH in rats by monocrotaline injection. Tissue analysis, echocardiography, and ^{68}Ga-NOTA-MSA PET were performed weekly in rats after monocrotaline injection and in those treated with either sildenafil or macitentan. The translational potential of ^{68}Ga-NOTA-MSA PET was explored in PAH patients.

Measurements and Main Results: Gene sets related to macrophages were significantly enriched on whole transcriptome sequencing of the lung tissue in PAH rats. Serial PET images of PAH rats demonstrated increasing uptake of ^{68}Ga-NOTA-MSA in the lung by time, that corresponded with the MR-positive macrophage recruitment observed in immunohistochemistry. In sildenafil- or macitentan-treated PAH rats, the infiltration of MR-positive macrophages by histology and the uptake of ^{68}Ga-NOTA-MSA on PET was significantly lower than that of the PAH-only group. The pulmonary uptake of ^{68}Ga-NOTA-MSA was significantly higher in PAH patients than normal subjects (p=0.009) or than those with pulmonary hypertension by left heart disease (p=0.019) (n=5 per group).

Conclusions: ^{68}Ga-NOTA-MSA PET can help diagnose PAH and monitor the inflammatory status by imaging the degree of macrophage infiltration into the lung. These observations suggest that ^{68}Ga-NOTA-MSA PET has the potential to be used as a novel noninvasive

diagnostic and monitoring tool of PAH.

Number of words in the abstract: 250

Key Words: pulmonary artery hypertension, molecular imaging, macrophage, diagnosis, monitoring

AJRCCM Articles in Press. Published on 19-July-2019 as 10.1164/rccm.201903-0639OC

INTRODUCTION

Pulmonary artery hypertension (PAH) is a complex and debilitating group of diseases characterized by hyper-proliferative remodeling of pulmonary vessels that leads to an increase in pulmonary vascular resistance, excessive afterload on the right ventricle (RV), and ultimately, the risk of RV failure and death (1). An important clinical feature of PAH is that its symptoms and signs are nonspecific, which hampers early diagnosis and timely treatment. Unfortunately, current diagnostic tools, such as right heart catheterization and echocardiography, cannot reliably identify patients with early stage PAH, either because they are too invasive for common use or because they are not accurate enough (2). Despite the fact that early detection of PAH progression leads to better outcomes (3, 4), it has been reported that current noninvasive diagnostic techniques are not suitable for monitoring the response to PAH treatment (5), leaving a huge unmet clinical need. These difficulties also preclude the appropriate initiation and adjustment of PAH therapy and it is one of the main reasons for the poor prognosis of PAH patients (2).

Among the several pathophysiological mechanisms of PAH (6-8), there have been intense attention on the role of altered immune process and failure to resolve inflammation in PAH patients (9). Among various immune effector cells in PAH, there are multiple lines of evidence that macrophages may play an important role in the development and progression of PAH. Specifically, several experimental and clinical studies consistently show that macrophage infiltration is prominent in animal models of PAH and in PAH patients (9-11). Early recruitment and activation of mannose receptor (MR)-positive macrophages have been found to be essential for the development of PAH animal models (12) and also to be increased in the lungs of idiopathic PAH patients (13). Furthermore, previous research showed that depletion or inactivation of macrophages could prevent or reverse PAH (14). Collectively, these observations suggest that molecular imaging of MR-positive macrophages

in the lungs can be used for the diagnosis and treatment monitoring of PAH by imaging the inflammatory status of the lungs.

We have recently shown that imaging of MR-positive macrophages may be promising for monitoring myocarditis, using positron emission tomography (PET)/computed tomography (CT) scan with ^{68}Ga-2-(*p*-isothiocyanatobenzyl)-1,4,7-triazacyclononane-1,4,7-triacetic acid (NOTA) mannosylated human serum albumin (MSA), a tracer targeting the MR (15). In the present study, we hypothesized that the recruitment of macrophages into the lung vasculature can be harnessed to accurately evaluate PAH using ^{68}Ga-NOTA-MSA PET/CT scan. We tested this hypothesis in animal PAH models and explored the translational potential in PAH patients.

AJRCCM Articles in Press. Published on 19-July-2019 as 10.1164/rccm.201903-0639OC

METHODS

For details on METHODS, see Supplemental Methods.

Ethics statements of animal studies

All animal experimental protocol was approved by the Institutional Animal Care and Use Committee (IACUC) of Seoul National University Hospital (IACUC No. 14-0215-C1A0). The experiments also comply with the Guide for the Care and Use of Laboratory Animals (National Research Council, revised in 2011). Animal studies using radioactive tracers were approved by the local Institutional Biosafety Committee.

Transcriptome sequencing and data analysis

We examined the whole transcriptomic profile of the rat lung tissues collected after 1, 2, 3 weeks of subcutaneous monocrotaline administration (n=3 per group of each week) and compared them with controls (n=3). The lung tissues were processed and the RNA quality checked, quantified, and sequenced as previously described (16). We focused on macrophage-related biological processes enriched with genes identified from *t*-test, using the annotations defined by the Gene Ontology (GO) Consortium. The enrichments of gene clusters in GO terms were assessed using a gene set enrichment test to compare the number of genes in each cluster associated with the studied meta-data to its expected value in the whole genome (12,750 genes). The hyper-geometric *p* value was calculated as the probability of more occurrences of a term in a study set compared to the number of occurrences of that term in the background set.

Rat model of PAH

Pulmonary hypertension (PH) was induced in 6-week old female Sprague-Dawley rats by an

intraperitoneal single injection of monocrotaline (60mg/kg, Sigma-Aldrich, MO), with ^{68}Ga-NOTA-MSA PET/CT scans and echocardiograms weekly thereafter. The degree of RV hypertrophy was expressed as the Fulton index, which is the weight ratio of RV divided by the sum of left ventricle and septum.

Assessment of specificity of ^{68}Ga-NOTA-MSA tracer for MR

To validate the feasibility of ^{68}Ga-NOTA-MSA PET/CT assessment and its specificity to MR, biodistribution analysis of ^{68}Ga-NOTA-MSA was performed in 10-week old female BALB/c mice and also, in PAH rats. ^{68}Ga-NOTA-MSA was prepared as previously described (17). Mannan solution (25mg/mL) was used as a MR blocker.

^{68}Ga-NOTA-MSA PET/CT image acquisition and analysis

PET images were obtained by list mode in isoflurane-anaesthetized rats, for 60 minutes after intravenous administration of ^{68}Ga-NOTA-MSA (55.5MBq) using a small-animal PET/CT scanner (eXplore VISTA, GE Healthcare, WI). Based on a pilot analysis of dynamic images, static PET images were reconstructed using images acquired during 40–60 minutes post-injection (Figure E1). Image reconstruction was conducted as described previously (15). The degree of ^{68}Ga-NOTA-MSA uptake were measured by drawing regions of interest (ROI) at the lung and the reference tissue (paraspinal muscle) on the co-registered trans-axial PET/CT images (Figure E2), and the degree of ^{68}Ga-NOTA-MSA uptake in the lung was presented as the lung-to-reference ratio (LRR). The paraspinal muscle was selected as the reference tissue in this animal experiment, since in rats, the superior vena cava (SVC) was too small to serve as the reference.

Human studies

AJRCCM Articles in Press. Published on 19-July-2019 as 10.1164/rccm.201903-0639OC

Human studies were conducted in accordance with the latest Declaration of Helsinki and the study protocol was reviewed and approved by the Institutional Review Board (IRB) of Seoul National University Hospital (IRB No. 1506-156-686). All subjects gave written informed consent for study enrollment. From April 2014, we prospectively recruited 5 patients with idiopathic PAH or connective tissue disease-related PAH, who were confirmed by cardiac catheterization. The diagnosis of PAH was based on the standard definition of mean PAP≥25mmHg, pulmonary artery wedge pressure (PAWP)≤15mmHg, and pulmonary vascular resistance (PVR)>3 wood unit (1, 5). Five healthy volunteers served as a normal control group. Five patients with PH due to left heart disease (PH-LHD) served as another control group. Major exclusion criteria are listed separately (Table E1).

The ^{68}Ga-NOTA-MSA PET/CT images were batch-analyzed by an investigator blinded to the clinical and hemodynamic data of the study participants. The ROIs were drawn for lungs and the reference tissue (SVC) (18), and the degree of uptake in the lungs were expressed as the LRR.

Statistical analysis

Continuous and categorical data were presented as median (range) and number (percent), respectively. The Student t test or Mann-Whitney U test was used to compare continuous variables, and the Chi-square test or Fisher's exact test was used to compare categorical variables as appropriate. One-way analysis of variance (ANOVA) followed by Bonferroni post-hoc test was performed for comparisons between multiple groups. In cases where the data was not normally distributed, Kruskal-Wallis test followed by Dunn's multiple comparison test was used to compare the mean ranks. In circumstances when the clustered nature of data (i.e., more vessels within the same rat) should be considered, the generalized estimating equation approach was used for the comparison between groups. For analyses of

gene expression data, the false discovery rate was controlled by adjusting p-value using Benjamini-Hochberg algorithm. Spearman's ρ was used to quantify the correlations between variables. Statistical analysis was performed with SPSS version 23.0 (SPSS Inc., IL). A two-sided *p* value <0.05 was considered significant.

AJRCCM Articles in Press. Published on 19-July-2019 as 10.1164/rccm.201903-0639OC

RESULTS

Gene expression profiles of the lung in PAH

To demonstrate the importance of macrophages in the development of PAH, we investigated the whole transcriptomic profile of the rat lung tissues collected weekly after monocrotaline administration. We aimed to identify the GO categories enriched in the development of PAH by comparing the transcriptomic profile with the whole transcriptome background. The gene sets that were significantly enriched were the GO term "Positive regulation of macrophage migration", "Positive regulation of macrophage activation", and "Macrophage activation involved in immune response" (hyper-geometric p=0.0003, 0.0045, and 0.0379, respectively; **Figure 1A**). The transcriptomic level of the *MRC1*, the gene coding MR, gradually increased (p<0.001 by ANOVA), with the difference becoming significant at 3 weeks after monocrotaline injection compared with the normal controls (p<0.001; **Figure 1B**).

Specificity of ^{68}Ga-NOTA-MSA for MR

The biodistribution assay showed a significantly lower uptake of ^{68}Ga-NOTA-MSA in the liver of mice by MR blockade, i.e. lower radioactivity in the liver of group 1 (MR blockade with high-dose mannan) and group 2 (MR blockade with low-dose mannan) than the control, group 3 (no MR blockade) (**Figure 2**). Specifically, the administration of mannan produced a dose-dependent reduction in the liver uptake of ^{68}Ga-NOTA-MSA, and compared with group 3, group 1 and 2 had a significantly reduced ^{68}Ga-NOTA-MSA uptake with a 46% and 34% decrease at 10 minutes, a 61% and 54% decrease at 1 hour, and a 57% and 43% decrease at 2 hours post-injection, respectively (**Figure 2A**). **Figure 2B** shows the representative ^{68}Ga-NOTA-MSA PET scans of mice in group 1, 2, and 3. When the same set of experiments were done with the PAH rats, the LRR was significantly lower in the MR blockade PAH rats than in the PAH only rats (10.94±3.29 for MR blockade PAH rats versus 15.95±4.09 for PAH

only rats; p=0.039; n=5 per group).

Association of ^{68}Ga-NOTA-MSA uptake with PAH progression

We assessed the uptake of ^{68}Ga-NOTA-MSA in the lung weekly after the monocrotaline injection (**Figure 3A**). Monocrotaline injection resulted in progressive pulmonary vascular remodeling, characterized by narrowing or obliteration of the lumen that became prominent between week 2 and 3 (upper panel of Figure E2A). The lung tissue demonstrated increasing infiltration of the ED1-positive macrophages (lower panel of Figure E2A) and the MR-positive macrophages around the pulmonary arterioles (**Figure 3B**), with the difference becoming pronounced starting from week 1 after monocrotaline injection. The percent wall thickness, the number of MR-positive macrophages, and the Fulton index increased as PAH evolved over 3 weeks; the difference in MR-positive macrophage number and the Fulton index became significant starting from week 1 following monocrotaline injection whereas the increase in the percent wall thickness was significant from week 2 (**Figure 3C-E**). The pulmonary artery acceleration time (PAAT), a parameter that inversely correlates with the mean pulmonary artery pressure (PAP) (19), gradually decreased (**Figure 3F** and Figure E2B) as PAH evolved. Serial PET images showed an increasing uptake of ^{68}Ga-NOTA-MSA in the lung that reached significantly higher levels than the control animals at the 1-week time point after monocrotaline injection (**Figure 3G-H**). The lung uptake of ^{68}Ga-NOTA-MSA correlated with the degree of lung infiltration of the MR-positive macrophages (Spearman's ρ=0.883, p<0.001) (**Figure 3I**). The correlations of ^{68}Ga-NOTA-MSA uptake with other PAH parameters are presented in Table E2. The biodistribution assay in post-mortem animals also supported the increased ^{68}Ga-NOTA-MSA uptake in the lung (Table E3).

Decline of ^{68}Ga-NOTA-MSA uptake after PAH-targeted therapy

AJRCCM Articles in Press. Published on 19-July-2019 as 10.1164/rccm.201903-0639OC

We assessed the lung uptake of ^{68}Ga-NOTA-MSA in the PAH rats after treatment with either sildenafil or macitentan, the two commonly used targeted agents for PAH (**Figure 4A**). In contrast to the PAH-only rats, the increase in the degree of pulmonary arteriolar muscularization, infiltration of MR-positive macrophages, and the Fulton index was significantly attenuated in rats treated with either sildenafil or macitentan (**Figure 4B-E** and Figure E4). The decrease in PAAT was restored by treatment with either sildenafil or macitentan (**Figure 4F**). The ^{68}Ga-NOTA-MSA PET showed that the uptake of the tracer in the lung was significantly lower in the sildenafil- and macitentan-treated groups than the PAH-only group (**Figure 4G-H**), a pattern similar to that histologically observed in the infiltration of MR-positive macrophages.

Human application of ^{68}Ga-NOTA-MSA in PAH patients

^{68}Ga-NOTA-MSA PET/CT was performed in patients with PAH, PH-LHD, and normal subjects (n=5 in each group). None of the participants complained of any symptoms or signs of adverse events after ^{68}Ga-NOTA-MSA administration. Baseline characteristics of the study participants are summarized in Table 1. There was no significant difference in age, sex, and body mass index between normal subjects and patients with PAH. Patients with PH-LHD were significantly older than those with PAH (58.0 [51.5-70.5] vs. 36.0 [23.0-51.5] years, p=0.032), with no difference in sex distribution nor in the anthropometric parameters between the groups. The mean PAP and PVR was not significantly different between PAH patients versus PH-LHD patients (54.0 [33.5-63.5] vs. 44.0 [36.5-52.0] mmHg, p=0.690 for mean PAP; 16.6 [8.8-18.4] vs. 6.6 [2.83- 8.8] WU, p=0.056 for PVR). The median interval between cardiac catheterization and ^{68}Ga-NOTA-MSA PET/CT scan was 6 days for PAH patients and 11 days for PH-LHD patients, respectively, which were not statistically different. Only one patient with PAH underwent ^{68}Ga-NOTA-MSA PET/CT 6 months after cardiac

catheterization due to a conflict in the personal schedule, but no significant aggravation or improvement of PAH was evident during this interval. Detailed data of the individual participants are listed in Table E4 and E5.

The degree of ^{68}Ga-NOTA-MSA uptake in the lung was significantly higher in the PAH patients than the normal subjects (p=0.011) or the patients with PH-LHD (p=0.008) (**Figure 5A**). The results remained significant when one patient who underwent ^{68}Ga-NOTA-MSA PET/CT 6 months after cardiac catheterization was excluded from the analysis (p=0.034 and p=0.042, respectively). The representative ^{68}Ga-NOTA-MSA PET/CT scans of two patients with PAH, one patient with PH-LHD, and one normal subject is shown (**Figure 5C-F**). In PAH patients, the ^{68}Ga-NOTA-MSA uptake pattern was mainly diffuse in both lung fields with more pronounced uptake in the central portion (**Figure 5C-D**). There was no significant ^{68}Ga-NOTA-MSA uptake in the lung of the patients with PH-LHD, except for the focal uptake along the lesion corresponding to a localized bronchiectasis (**Figure 5E**). No ^{68}Ga-NOTA-MSA lung uptake was evident in the normal subjects (**Figure 5F**).

In the subgroup of PAH patients, the LRR did not significantly correlate with the invasively measured hemodynamic parameters (**Table 2**), suggesting that the degree of ^{68}Ga-NOTA-MSA uptake in the lung targets a process that is different from the hemodynamic process of the PAH development. There was also no significant correlation between LRR and various hemodynamic parameters in the subgroup of PH-LHD patients.

AJRCCM Articles in Press. Published on 19-July-2019 as 10.1164/rccm.201903-0639OC

DISCUSSION

The major findings of our study can be summarized as follows: 1) the expression of genes related to macrophages, such as *MRC1*, are increased in MCT-induced PAH rats, as revealed by transcriptome analysis, 2) ^{68}Ga-NOTA-MSA is specific for MR, suggesting that this PET tracer binds to MR-expressing cells, such as macrophages, 3) the increase in pulmonary ^{68}Ga-NOTA-MSA uptake on PET/CT occurred 1 to 3 weeks after monocrotaline injection, suggesting that this novel molecular imaging technique may enable the detection of PAH earlier before the change in hemodynamic parameters, 4) treatment with sildenafil or macitentan significantly decreased the lung uptake of ^{68}Ga-NOTA-MSA, which supports that this technology may have the potential applications to assess the response to PAH-specific therapy, and 5) human studies demonstrated that the lung uptake of ^{68}Ga-NOTA-MSA was increased in PAH patients, but neither in normal subjects nor in patients with PH-LHD, suggesting its specificity. These findings demonstrate that the measurement of lung ^{68}Ga-NOTA-MSA uptake makes it possible to noninvasively and quantitatively visualize the recruitment of MR-positive macrophage to the pulmonary vasculature in PAH patients for the purpose of adequate diagnosis and monitoring of PAH.

Although various types of inflammatory cells are implicated in PAH, macrophages have been reported to be particularly associated with this disease process (20, 21). Our study also supports the role of macrophages in PAH, by showing that gene sets related to macrophage migration and activation were significantly enriched in the transcriptomic analysis of the PAH lung tissues. This finding is plausible given that the monocrotaline model is a toxic inflammatory model of PAH (22). Since this study primarily focused on the diagnostic utility of ^{68}Ga-NOTA-MSA imaging, we did not assess whether an increased presence and activity of macrophages were observed in other animal models of PAH. However, previous studies suggest that macrophages may play an essential role in pulmonary

vascular remodeling in animal models of hypoxia-induced PAH and portopulmonary hypertension (10). Furthermore, considering that the inflammatory component of human PAH is best resembled by the monocrotaline-induced PAH rat model (23), this animal model may be the most appropriate model for translation of research findings on inflammation in PAH into humans.

Among the different subsets of macrophages, M2 macrophages have been recognized as a key contributor to pulmonary vascular remodeling, possibly via the secretion of Fizz1, a molecule with mitogenic, profibrotic, and vasoconstrictive properties (24, 25). One previous study showed that early recruitment of M2 macrophages is crucial for the development of PAH, suggesting that the assessment of M2 activation may serve as a potential tool for early diagnosis and disease progression monitoring of PAH (12). This is also supported by a human study showing that the expression of MR, one of the most widely used markers of M2 macrophages, was observed *in vivo* in idiopathic PAH patients (26). Our study demonstrated that the uptake of ^{68}Ga-NOTA-MSA was blocked by the administration of mannan, a MR-specific antagonist, suggesting that ^{68}Ga-NOTA-MSA imaging can be used to specifically detect the recruitment of macrophages expressing MR.

Previous studies suggested that fluorine-18–labeled 2-fluoro-2-deoxyglucose (^{18}F-FDG) PET may be useful as an imaging tool to assess the molecular pathology of PAH and its diagnosis and monitoring (19, 27). Considering that ^{18}F-FDG uptake generally reflects glucose metabolism in both proliferative and inflammatory cells, ^{18}F-FDG PET may not image the inflammatory processes specifically. In contrast, the ^{68}Ga-NOTA-MSA uptake followed the degree of macrophage infiltration, suggesting its specificity for monitoring the status of inflammatory cell infiltration and a different standpoint of understanding the process of PAH. Therefore, it is possible that the use of ^{68}Ga-NOTA-MSA can be helpful in the identification of subgroups of PAH patients who might most benefit from treatments mainly

AJRCCM Articles in Press. Published on 19-July-2019 as 10.1164/rccm.201903-0639OC

targeting the inflammatory pathways.

Notably, the uptake of ^{68}Ga-NOTA-MSA was significantly higher in patients with PAH than those with PH-LHD. Because the differentiation of PAH from PH-LHD remains a practical challenge, especially without the use of invasive catheterization, ^{68}Ga-NOTA-MSA PET imaging might be promising as a noninvasive tool for this purpose. Although speculative, combined post- and pre-capillary PH could include inflammatory change to the left ventricle depending on the associated disease in a given patient (15, 28), and this finding might help identify combined pre/post-capillary PAH. However, further studies are clearly required to validate and extend our finding concerning the role of ^{68}Ga-NOTA-MSA PET imaging in the diagnosis and differentiation of PAH from other forms of PH. On the other hand, we did not find a significant correlation between LRR and various hemodynamic parameters in both the subgroup of PAH and PH-LHD, suggesting that ^{68}Ga-NOTA-MSA may be more reflective of inflammatory status rather than obliteration of the pulmonary vascular bed and resultant RV pressure overload (Figure E5). Considering that soluble CD163, a macrophage activation marker, has been recently described as a promising serum marker of inflammatory status in several patient population (29-31), the measurement of the inflammatory status by ^{68}Ga-NOTA-MSA PET may provide further insight into the clinical relevance of this imaging modality.

In the present study, SVC was used as the reference region for uptake measurement, since it has been preferred in several previous studies (32, 33). Although the pulmonary artery might be more robust against partial volume effect than SVC due to larger size, veins have been generally preferred to arteries because there may be some uptake of tracers in the arterial muscle cells. Furthermore, in the setting of PAH, with possible progression to dilatation of the lumen or the hypertrophy of arterial/ventricular wall, there are concerns with any unexpected influence of PAH on the measurement of uptake in pulmonary artery, right

ventricle, and right atrium, making them difficult to be used as the reference region.

Recent evidence indicates that a comprehensive risk stratification at early stage may determine the prognosis in PAH patients (34, 35). The adequate assessment of response to initial therapy allows timely decision of maintaining initial therapy or changing to combination therapy, consequently leading to better treatment outcomes. Our study demonstrated that the uptake of ^{68}Ga-NOTA-MSA decreased in PAH rats treated with either sildenafil or macitentan, compared with those receiving vehicle only. This finding is in line with previous studies showing that phosphodiesterase type 5 inhibitors or endothelin receptor antagonists could attenuate the recruitment or activation of macrophages into various tissues, including adipose tissue, renal parenchyma, or atherosclerotic plaque (36-38). We did not explore the mechanism of macrophage-inhibiting effects of these agents, because this study focused on whether ^{68}Ga-NOTA-MSA PET imaging can detect treatment response consistent with the findings of *ex vivo* experiments. However, our study suggests that this molecular imaging technique has the potential of contributing to a more comprehensive assessment of treatment response during follow-up of PAH patients, by providing information on the change in inflammatory activity in addition to the variables reflecting symptomatic, functional, and hemodynamic status, information that is not at all provided by the current state-of-art evaluation techniques.

Study Limitations

First, because of the small number of participants, our findings do not allow a generalized conclusion in human subjects. It is also difficult to conclude on a confident relationship between the degree of ^{68}Ga-NOTA-MSA uptake and the hemodynamic severity of PAH. Further studies with larger number of patients are warranted to validate our findings. Second, we did not have follow-up data on the changes in lung uptake of ^{68}Ga-NOTA-MSA in PAH

AJRCCM Articles in Press. Published on 19-July-2019 as 10.1164/rccm.201903-0639OC

patients after PAH-specific therapies. Although our results from animal experiments suggest that ^{68}Ga-NOTA-MSA PET/CT has the potential of monitoring the treatment response to PAH-targeted therapy, further investigation is necessary to investigate whether this can be extrapolated to PAH patients. Third, transcriptomic analysis of whole lung tissue may confound the determination of the cell type and the biological pathways associated with PAH, since the result of this analysis is influenced by the changes in the cellular composition of the tissue (39). Fourth, we did not assess the changes in pulmonary blood volume or flow induced in the monocrotaline model, a factor that can affect tracer delivery to the lungs. If monocrotaline per se reduces pulmonary blood flow and thus tracer delivery to the lungs, it can potentially confound interpretation of pulmonary ^{68}Ga-NOTA-MSA uptake. However, it has been suggested that pulmonary blood flow is not significantly changed by monocrotaline injection (40). Lastly, the optimal method for measuring pulmonary ^{68}Ga-NOTA-MSA uptake is unclear. Although there is no data yet to support that the target-to-background ratio is reliable for assessing ^{68}Ga-NOTA-MSA uptake as in ^{18}F-FDG uptake, the target-to-background ratio, such as LRR used in our study, is a widely used, reproducible method to evaluate the tissue uptake of the radiotracer with an excellent correlation with histological markers of inflammation.

CONCLUSIONS

We demonstrate the possibility that ^{68}Ga-NOTA-MSA PET imaging can be valuable for noninvasive assessment of inflammatory status in PAH, by visualizing the infiltration of macrophages into the lungs. This novel imaging technology may also hold promise for an improved assessment of treatment response to PAH-targeted therapy.

AT A GLANCE COMMENTARY

Scientific Knowledge on the Subject

Although it is well known that macrophages are effector cells that drives the progression of pulmonary artery hypertension (PAH), methods to assess the inflammatory cell infiltration using noninvasive imaging are largely lacking. The present study was inspired by the findings that ^{68}Ga-2-(*p*-isothiocyanatobenzyl)-1,4,7-triazacyclononane-1,4,7-triacetic acid (NOTA) mannosylated human serum albumin (MSA), a tracer targeting the mannose receptor on macrophages, may have a potential to evaluate macrophage infiltration in PAH.

What This Study Adds to the Field

We hypothesized that macrophage recruitment into the lung vasculature can be harnessed to assess PAH using ^{68}Ga-NOTA-MSA positron emission tomography (PET) and tested this hypothesis in animal PAH models and in patients with PAH. The increase in pulmonary ^{68}Ga-MSA-NOTA uptake on PET occurs 1 to 3 weeks after monocrotaline injection, suggesting that this molecular imaging technique enables the detection of PAH earlier before hemodynamic changes. Treatment with sildenafil or macitentan significantly reduces the pulmonary ^{68}Ga-MSA-NOTA uptake, supporting that this technology may have potential applications to monitor the response to PAH-specific therapy. Finally, the pulmonary ^{68}Ga-MSA-NOTA uptake is increased in PAH patients, but neither in normal subjects nor in patients with pulmonary hypertension due to left heart disease, suggesting its translational potential.

ACKNOWLEDGEMENTS: We thank Mi-Kyung Hong, RDCS and Narae Park, RDCS for the echocardiography, Mi Kyeong Hong, MS for the synthesis of the ^{68}Ga-NOTA-MSA, and Young Ju Kim, BS for the help in the biodistribution assays.

AJRCCM Articles in Press. Published on 19-July-2019 as 10.1164/rccm.201903-0639OC

REFERENCES

1. Simonneau G, Gatzoulis MA, Adatia I, Celermajer D, Denton C, Ghofrani A*, et al.* Updated clinical classification of pulmonary hypertension. *J Am Coll Cardiol* 2013;62:D34-41.

2. Lau EM, Humbert M, Celermajer DS. Early detection of pulmonary arterial hypertension. *Nat Rev Cardiol* 2015;12:143-155.

3. Humbert M, Sitbon O, Chaouat A, Bertocchi M, Habib G, Gressin V*, et al.* Survival in patients with idiopathic, familial, and anorexigen-associated pulmonary arterial hypertension in the modern management era. *Circulation* 2010;122:156-163.

4. Galie N, Rubin L, Hoeper M, Jansa P, Al-Hiti H, Meyer G*, et al.* Treatment of patients with mildly symptomatic pulmonary arterial hypertension with bosentan (EARLY study): a double-blind, randomised controlled trial. *Lancet* 2008;371:2093-2100.

5. McLaughlin VV, Shah SJ, Souza R, Humbert M. Management of pulmonary arterial hypertension. *J Am Coll Cardiol* 2015;65:1976-1997.

6. Rabinovitch M. Molecular pathogenesis of pulmonary arterial hypertension. *J Clin Invest* 2012;122:4306-4313.

7. Thenappan T, Prins KW, Pritzker MR, Scandurra J, Volmers K, Weir EK. The Critical Role of Pulmonary Arterial Compliance in Pulmonary Hypertension. *Ann Am Thorac Soc* 2016;13:276-284.

8. van der Feen DE, Berger RMF, Bartelds B. Converging Paths of Pulmonary Arterial Hypertension and Cellular Senescence. *Am J Respir Cell Mol Biol* 2019.

9. Rabinovitch M, Guignabert C, Humbert M, Nicolls MR. Inflammation and immunity in the pathogenesis of pulmonary arterial hypertension. *Circ Res* 2014;115:165-175.

10. Thenappan T, Goel A, Marsboom G, Fang YH, Toth PT, Zhang HJ*, et al.* A central role for CD68(+) macrophages in hepatopulmonary syndrome. Reversal by macrophage depletion. *Am J Respir Crit Care Med* 2011;183:1080-1091.

11. Frid MG, Brunetti JA, Burke DL, Carpenter TC, Davie NJ, Reeves JT*, et al.* Hypoxia-induced pulmonary vascular remodeling requires recruitment of circulating mesenchymal precursors of a monocyte/macrophage lineage. *Am J Pathol* 2006;168:659-669.

12. Vergadi E, Chang MS, Lee C, Liang OD, Liu X, Fernandez-Gonzalez A*, et al.* Early macrophage recruitment and alternative activation are critical for the later development of hypoxia-induced pulmonary hypertension. *Circulation* 2011;123:1986-1995.

13. Hashimoto-Kataoka T, Hosen N, Sonobe T, Arita Y, Yasui T, Masaki T*, et al.* Interleukin-6/interleukin-21 signaling axis is critical in the pathogenesis of pulmonary arterial hypertension. *Proc Natl Acad Sci U S A* 2015;112:E2677-2686.

14. Tian W, Jiang X, Tamosiuniene R, Sung YK, Qian J, Dhillon G*, et al.* Blocking macrophage leukotriene b4 prevents endothelial injury and reverses pulmonary hypertension. *Sci Transl Med* 2013;5:200ra117.

15. Lee SP, Im HJ, Kang S, Chung SJ, Cho YS, Kang H*, et al.* Noninvasive Imaging of Myocardial Inflammation in Myocarditis using 68Ga-tagged Mannosylated Human Serum Albumin Positron Emission Tomography. *Theranostics* 2017;7:413-424.

16. Baek A, Cho SR, Kim SH. Elucidation of Gene Expression Patterns in the Brain after Spinal Cord Injury. *Cell Transplant* 2017;26:1286-1300.

17. Choi JY, Jeong JM, Yoo BC, Kim K, Kim Y, Yang BY*, et al.* Development of 68Ga-labeled mannosylated human serum albumin (MSA) as a lymph node imaging agent for positron emission tomography. *Nuclear medicine and biology* 2011;38:371-379.

18. Rudd JH, Myers KS, Bansilal S, Machac J, Rafique A, Farkouh M*, et al.* (18)Fluorodeoxyglucose positron emission tomography imaging of atherosclerotic plaque inflammation is highly reproducible: implications for atherosclerosis therapy trials. *J Am Coll Cardiol* 2007;50:892-896.

AJRCCM Articles in Press. Published on 19-July-2019 as 10.1164/rccm.201903-0639OC

19. Marsboom G, Wietholt C, Haney CR, Toth PT, Ryan JJ, Morrow E*, et al.* Lung (1)(8)F-fluorodeoxyglucose positron emission tomography for diagnosis and monitoring of pulmonary arterial hypertension. *Am J Respir Crit Care Med* 2012;185:670-679.

20. Pinto RF, Higuchi Mde L, Aiello VD. Decreased numbers of T-lymphocytes and predominance of recently recruited macrophages in the walls of peripheral pulmonary arteries from 26 patients with pulmonary hypertension secondary to congenital cardiac shunts. *Cardiovasc Pathol* 2004;13:268-275.

21. Sahara M, Sata M, Morita T, Nakamura K, Hirata Y, Nagai R. Diverse contribution of bone marrow-derived cells to vascular remodeling associated with pulmonary arterial hypertension and arterial neointimal formation. *Circulation* 2007;115:509-517.

22. Gomez-Arroyo JG, Farkas L, Alhussaini AA, Farkas D, Kraskauskas D, Voelkel NF*, et al.* The monocrotaline model of pulmonary hypertension in perspective. *Am J Physiol Lung Cell Mol Physiol* 2012;302:L363-369.

23. Hoffmann J, Wilhelm J, Olschewski A, Kwapiszewska G. Microarray analysis in pulmonary hypertension. *Eur Respir J* 2016;48:229-241.

24. Angelini DJ, Su Q, Yamaji-Kegan K, Fan C, Skinner JT, Champion HC*, et al.* Hypoxia-induced mitogenic factor (HIMF/FIZZ1/RELMalpha) induces the vascular and hemodynamic changes of pulmonary hypertension. *Am J Physiol Lung Cell Mol Physiol* 2009;296:L582-593.

25. Teng X, Li D, Champion HC, Johns RA. FIZZ1/RELMalpha, a novel hypoxia-induced mitogenic factor in lung with vasoconstrictive and angiogenic properties. *Circ Res* 2003;92:1065-1067.

26. El Kasmi KC, Pugliese SC, Riddle SR, Poth JM, Anderson AL, Frid MG*, et al.* Adventitial fibroblasts induce a distinct proinflammatory/profibrotic macrophage phenotype in pulmonary hypertension. *J Immunol* 2014;193:597-609.

27. Zhao L, Ashek A, Wang L, Fang W, Dabral S, Dubois O*, et al.* Heterogeneity in lung (18)FDG uptake in pulmonary arterial hypertension: potential of dynamic (18)FDG positron emission tomography with kinetic analysis as a bridging biomarker for pulmonary vascular remodeling targeted treatments. *Circulation* 2013;128:1214-1224.

28. Elinoff JM, Agarwal R, Barnett CF, Benza RL, Cuttica MJ, Gharib AM*, et al.* Challenges in Pulmonary Hypertension: Controversies in Treating the Tip of the Iceberg. A Joint National Institutes of Health Clinical Center and Pulmonary Hypertension Association Symposium Report. *Am J Respir Crit Care Med* 2018;198:166-174.

29. Kazankov K, Barrera F, Moller HJ, Bibby BM, Vilstrup H, George J*, et al.* Soluble CD163, a macrophage activation marker, is independently associated with fibrosis in patients with chronic viral hepatitis B and C. *Hepatology* 2014;60:521-530.

30. Moller HJ, Frikke-Schmidt R, Moestrup SK, Nordestgaard BG, Tybjaerg-Hansen A. Serum soluble CD163 predicts risk of type 2 diabetes in the general population. *Clin Chem* 2011;57:291-297.

31. Etzerodt A, Berg RM, Plovsing RR, Andersen MN, Bebien M, Habbeddine M*, et al.* Soluble ectodomain CD163 and extracellular vesicle-associated CD163 are two differently regulated forms of 'soluble CD163' in plasma. *Sci Rep* 2017;7:40286.

32. Iwatsuka R, Matsue Y, Yonetsu T, O'Uchi T, Matsumura A, Hashimoto Y*, et al.* Arterial inflammation measured by (18)F-FDG-PET-CT to predict coronary events in older subjects. *Atherosclerosis* 2018;268:49-54.

33. Joseph P, Ishai A, Mani V, Kallend D, Rudd JH, Fayad ZA*, et al.* Short-term changes in arterial inflammation predict long-term changes in atherosclerosis progression. *Eur J Nucl Med Mol Imaging* 2017;44:141-150.

34. Kylhammar D, Kjellstrom B, Hjalmarsson C, Jansson K, Nisell M, Soderberg S*, et al.* A comprehensive risk stratification at early follow-up determines prognosis in pulmonary

AJRCCM Articles in Press. Published on 19-July-2019 as 10.1164/rccm.201903-0639OC

arterial hypertension. *Eur Heart J* 2017.

35. Douschan P, Kovacs G, Avian A, Foris V, Gruber F, Olschewski A*, et al.* Mild Elevation of Pulmonary Arterial Pressure as a Predictor of Mortality. *Am J Respir Crit Care Med* 2018;197:509-516.

36. Handa P, Tateya S, Rizzo NO, Cheng AM, Morgan-Stevenson V, Han CY*, et al.* Reduced vascular nitric oxide-cGMP signaling contributes to adipose tissue inflammation during high-fat feeding. *Arterioscler Thromb Vasc Biol* 2011;31:2827-2835.

37. Tullos NA, Stewart NJ, Davidovich R, Chade AR. Chronic blockade of endothelin A and B receptors using macitentan in experimental renovascular disease. *Nephrol Dial Transplant* 2015;30:584-593.

38. Babaei S, Picard P, Ravandi A, Monge JC, Lee TC, Cernacek P*, et al.* Blockade of endothelin receptors markedly reduces atherosclerosis in LDL receptor deficient mice: role of endothelin in macrophage foam cell formation. *Cardiovasc Res* 2000;48:158-167.

39. Reyfman PA, Walter JM, Joshi N, Anekalla KR, McQuattie-Pimentel AC, Chiu S*, et al.* Single-Cell Transcriptomic Analysis of Human Lung Provides Insights into the Pathobiology of Pulmonary Fibrosis. *Am J Respir Crit Care Med* 2018.

40. Chen EP, Bittner HB, Craig DM, Davis RD, Jr., Van Trigt P, 3rd. Pulmonary hemodynamics and blood flow characteristics in chronic pulmonary hypertension. *Ann Thorac Surg* 1997;63:806-813.

FIGURE LEGENDS

Figure 1. Transcriptome analysis of the PAH evolution.

(A) Heat map of the normalized transcriptome expression profile for control and monocrotaline-treated rats at 1, 2, and 3 weeks post-injection. Expression values are colored based on their z-score normalized FPKM values for each gene: yellow, relatively high transcript expression; blue, relatively low expression. Gene ontology terms "positive regulation of macrophage migration", "positive regulation of macrophage activation", and "macrophage activation involved in immune response" were significantly over-represented in the set of transcripts differentially expressed among the 4 groups (n=3 per group). **(B)** Comparison of the expression level of *MRC1* between the control and the monocrotaline-treated rats. FPKM=fragments per kilobase of exon model per million reads mapped.

Figure 2. In vivo biodistribution assay of ^{68}Ga-NOTA-MSA.

(A) Comparison of liver uptake of ^{68}Ga-NOTA-MSA between different groups of mice (n=4 per group). Group 1 indicates mice receiving ^{68}Ga-NOTA-MSA (24μCi) with MR blockade by high-dose mannan (2,500μg/animal); group 2 indicates mice receiving ^{68}Ga-NOTA-MSA (24μCi) with MR blockade by low-dose mannan (500μg/animal); and group 3 indicates mice receiving ^{68}Ga-NOTA-MSA (24μCi) without MR blockade. **(B)** Representative ^{68}Ga-NOTA-MSA PET images for each group. A high uptake of ^{68}Ga-NOTA-MSA in the liver was found in the mouse of group 3, whereas the uptake was substantially reduced in group 1 and 2. The color scale bar indicates the concentrations of radioactivity (Becquerel per volume of tissue, Bq/mL).

Figure 3. Time course of PAH progression and lung ^{68}Ga-NOTA-MSA uptake in PET after monocrotaline injection.

AJRCCM Articles in Press. Published on 19-July-2019 as 10.1164/rccm.201903-0639OC

(A) Schematic diagram of animal experiment. Timeline of PAH development in 6-week old female Sprague-Dawley rats and serial imaging with NOTA-MSA PET/CT scans and echocardiograms. **(B)** Histological changes of the lung in PAH progression. Note prominent infiltration of CD206 (MR)-positive macrophages around the pulmonary arteriole at 1, 2, and 3 weeks after monocrotaline administration. **(C-D)** There was a gradual and significant increase in percent wall thickness **(C)** and MR-positive macrophages per vessel **(D)** with PAH progression. Percent wall thickness was calculated by the ratio of medial wall thickness to the external diameter of small muscular pulmonary arterioles (≤150μm outer diameter) on hematoxylin and eosin (H&E)-stained lung sections. MR-positive macrophages near the pulmonary arterioles were counted. For each of the 4 groups, we measured 40 vessels per animal (n=8 per group). **(E)** A similar increment in the Fulton index (RV weight to left ventricle plus septum weight) was noted (n=8 per group). **(F)** PAAT was measured by Doppler echocardiography which decreased with the progression of PAH, a significant difference starting from week 2 (n≥10 per group). **(G-H)** Representative PET scans show increased ^{68}Ga-NOTA-MSA uptake in the lung fields of PAH rats **(G)**. Quantification of lung uptake of ^{68}Ga-NOTA-MSA demonstrates significantly higher uptake in PAH rats, starting from week 1 **(H)** (n≥10 per group). **(I)** There was a significant correlation between ^{68}Ga-NOTA-MSA uptake and degree of MR-positive macrophages per vessel. CT=computed tomography; IP=intraperitoneal; MCT=monocrotaline; MR=mannose receptor; MSA=mannosylated human serum albumin; NOTA=2-(p-isothiocyanatobenzyl)-1,4,7-triazacyclononane-1,4,7-triacetic acid; PAAT=pulmonary artery acceleration time. PET=positron emission tomography; SD=Sprague-Dawley.

Figure 4. Attenuation of the ^{68}Ga-NOTA-MSA uptake in the lung after treatment with sildenafil or macitentan.

(A) Schematic diagram of animal experiment. Timeline of treatment with sildenafil or macitentan after a single initial monocrotaline injection in rats. **(B)** Histological changes after 3-week oral administration of sildenafil (25mg/kg/day) or macitentan (30mg/kg/day) from the time of monocrotaline injection. Compared with the PAH rat without treatment, note the decrease of CD206 (MR)-positive macrophage infiltration around the pulmonary arteriole of the PAH rat treated with sildenafil or macitentan. **(C-D)** Treatment with sildenafil or macitentan attenuated monocrotaline-induced pulmonary arteriole muscularization **(C)** and CD206 (MR)-positive macrophage infiltration **(D)**. For each of the 4 groups, we measured 40 vessels per animal (n=5 per group). **(E-F)** Sildenafil or macitentan treatment partially improved the increased Fulton index **(E)** and the decreased PAAT induced by monocrotaline injection **(F)** (n=5 per group). **(G-H)** Representative PET scans demonstrate attenuation of ^{68}Ga-NOTA-MSA uptake in the lung of PAH rats treated with sildenafil or macitentan **(G)**. Quantification of lung ^{68}Ga-NOTA-MSA uptake shows that monocrotaline-induced increase of ^{68}Ga-NOTA-MSA uptake was attenuated with the administration of sildenafil or macitentan **(H)** (n≥5 per group). SIL-Tx=sildenafil-treated, MAC-Tx=macitentan-treated, other abbreviations as in Figure 3.

Figure 5. Application of ^{68}Ga-NOTA-MSA PET/CT imaging in patients with PAH.

(A) Quantification of lung ^{68}Ga-NOTA-MSA uptake demonstrates that patients with PAH had a significantly higher uptake than patients with PH-LHD or normal healthy subjects. **(B)** The lung ROI for each patient was segmented based on the Hounsfield unit (HU) of the CT image (-1000<HU<-200), as shown in the center panel. Red colored area in the right panel indicates the ROI used to assess lung uptake of ^{68}Ga-NOTA-MSA on PET images. **(C-F)** Representative ^{68}Ga-NOTA-MSA PET/CT images of the study participants. Diffusely increased lung uptake of ^{68}Ga-NOTA-MSA was observed in patients with PAH (**C**, Patient #14 and **D**, Patient #12).

AJRCCM Articles in Press. Published on 19-July-2019 as 10.1164/rccm.201903-0639OC

Only focal uptake of ^{68}Ga-NOTA-MSA in localized bronchiectasis was observed without increased uptake in the lung of a patient with PH-LHD (**E**, Patient #7). A representative negative ^{68}Ga-NOTA-MSA PET/CT scan image of a patient who did not have PH (**F**, Patient #5). The color scale bar indicates the lung-to-reference ratio. For details of patients' characteristics, see Table E4 and E5. PH-LHD=pulmonary hypertension due to left heart disease, PAH=pulmonary artery hypertension, PH=pulmonary hypertension.

TABLES

Table 1. Baseline Clinical, Hemodynamic, and ^{68}Ga-MSA-NOTA PET/CT Data of Study Participants

	Normal (n = 5)	PH-LHD (n = 5)	PAH (n = 5)	*p* normal vs. PAH	*p* PH-LHD vs. PAH
Age, years	44.0±7.0	60.4±10.1	37.0±15.0	0.421	0.032
	45.0 (37.5-50.0)	58.0 (51.5-70.5)	36.0 (23.0-51.5)		
Female	4 (80%)	3 (60%)	4 (80%)	1.000	0.490
Height, cm	163.4±12.0	163.8±10.5	160.6±7.8	0.841	0.690
	160.0 (154.8-173.7)	166.0 (153.0-173-5)	157.0 (154.0-169.0)		
Weight, kg	56.1±17.2	54.4±7.9	58.5±12.2	0.841	0.548
	49.0 (46.6-69.3)	53.0 (48.7-60.8)	62.0 (45.7-69.5)		
BMI, kg/m^2	20.7±3.3	20.2±2.2	22.9±3.8	0.421	0.222
	19.1 (18.4-23-8)	19.7 (18.2-22.5)	23.2 (19.2-26.4)		
BSA, m^2	1.60±0.28	1.56±0.15	1.62±0.20	0.690	0.841
	1.49 (1.43-1.82)	1.56 (1.42-1.72)	1.63 (1.46-1.79)		
SBP, mmHg	118.6±5.5	110.2±10.0	110.8±14.9	0.690	0.690

AJRCCM Articles in Press. Published on 19-July-2019 as 10.1164/rccm.201903-0639OC

	120.0 (114.0-122.5)	110.0 (101.0-119.5)	115.0 (95.5-121.0)		
DBP, mmHg	75.2±5.9	70.8±13.4	73.2±9.6	1.000	0.690
	75.0 (70.5-80.0)	70.0 (59.0-83.0)	75.0 (64.0-81.5)		
HR, bpm	78.8±7.0	84.8±11.5	79.6±15.8	0.841	0.690
	80.0 (72.0-85.0)	89.0 (73.5-94.0)	75.0 (66.5-95.0)		
SPAP, mmHg	-	69.8±19.5	71.8±22.5	-	0.841
		73.0 (50.5-87.5)	79.0 (48.0-92.0)		
DPAP, mmHg	-	26.8±8.6	34.8±11.9	-	0.421
		28.0 (19.5-33.5)	41.0 (22.0-44.5)		
MPAP, mmHg	-	44.2±9.2	49.6±15.3	-	0.690
		44.0 (36.5-52.0)	54.0 (33.5-63.5)		
PAWP, mmHg	-	24.6±12.0	11.6±3.8	-	0.008
		18.0 (17.0-35.5)	13.0 (8.5-14.0)		
TPG, mmHg		19.6±9.4	38.0±14.2		0.056
		22.0 (10.0-28.0)	40.0 (24.0-51.0)		
PVR, WU	-	6.0±3.2	14.2±5.7	-	0.056

		6.6 (2.8-8.8)	16.6 (8.8-18.4)		
PVRI, WU/m^2	-	9.2±4.8	23.3±10.1	-	0.056
		9.0 (4.7-13.7)	27.6 (12.9-31.4)		
CO, L/min	-	4.11±1.80	2.75±0.47	-	0.222
		3.53 (2.62-5.90)	2.70 (2.30-3.22)		
CI, L/min/m^2	-	2.58±1.01	1.80±0.46	-	0.222
		2.23 (1.78-3.55)	1.63 (1.54-2.15)		
Lung-to-reference ratio	0.18±0.01	0.18±0.02	0.26±0.05	0.011	0.008
	0.19 (0.17-0.19)	0.18 (0.16-0.20)	0.24 (0.23-0.31)		
Interval between RHC	-	10±7	43±81	-	1.000
and PET/CT, days		11 (3-17)	6 (4-101)		

Values given as number (percentage), mean±standard deviation, or median (interquartile range) unless otherwise indicated.

BMI, body mass index; BSA, body surface area; CI, cardiac index; CO, cardiac output; DBP, diastolic blood pressure; DPAP, diastolic pulmonary artery pressure; HR, heart rate; MPAP, mean pulmonary artery pressure; MSA, human serum albumin; PAH, pulmonary artery hypertension; PAWP, pulmonary artery wedge pressure; PET/CT, positron emission tomography/computed tomography; PH-LHD, PH due to left heart disease; PVR, pulmonary vascular resistance; PVRI, pulmonary vascular resistance index; RHC, right heart catheterization; SBP,

AJRCCM Articles in Press. Published on 19-July-2019 as 10.1164/rccm.201903-0639OC

systolic blood pressure; SPAP, systolic pulmonary artery pressure; TPG, transpulmonary pressure gradient.

TPG was calculated as the difference between MPAP and PAWP.

Table 2. Correlation of lung ^{68}Ga-NOTA-MSA uptake on PET scans with hemodynamic parameters measured by cardiac catheterization in patients with PAH or PH-LHD

	PAH		PH-LHD	
	Spearman's ρ	p	Spearman's ρ	p
SPAP	-0.400	0.505	-0.600	0.285
DPAP	-0.205	0.741	-0.200	0.747
MPAP	-0.400	0.505	-0.60	0.285
PAWP	0.872	0.054	-0.103	0.870
TPG	-0.400	0.505	-0.300	0.624
PVR	-0.100	0.873	0.200	0.747
PVRI	-0.400	0.505	0.200	0.747
CO	0.300	0.624	-0.100	0.873
CI	0.000	1.000	-0.300	0.624

Abbreviations are same as in Table 1.

AJRCCM Articles in Press. Published on 19-July-2019 as 10.1164/rccm.201903-0639OC

Figure 1

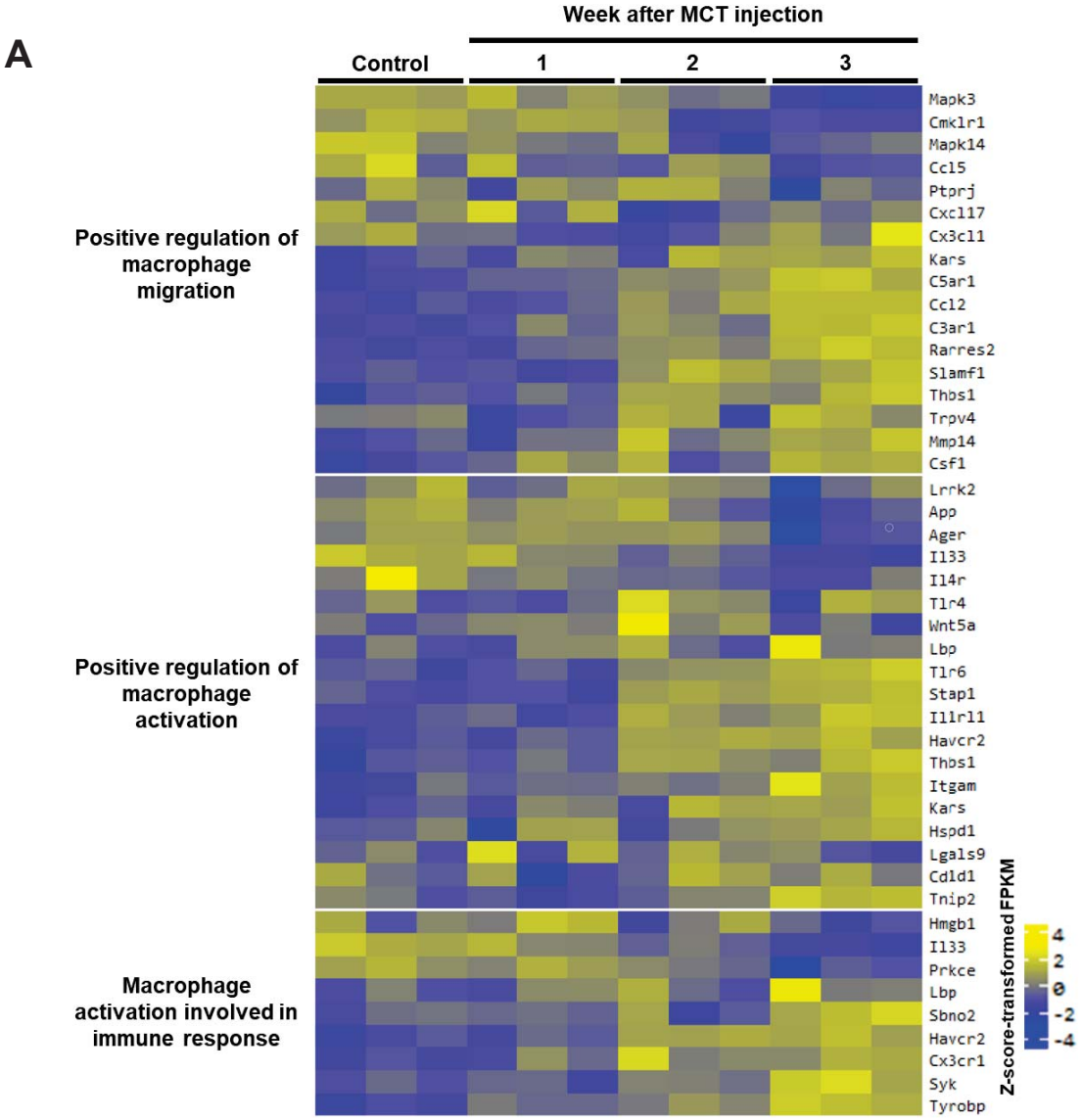

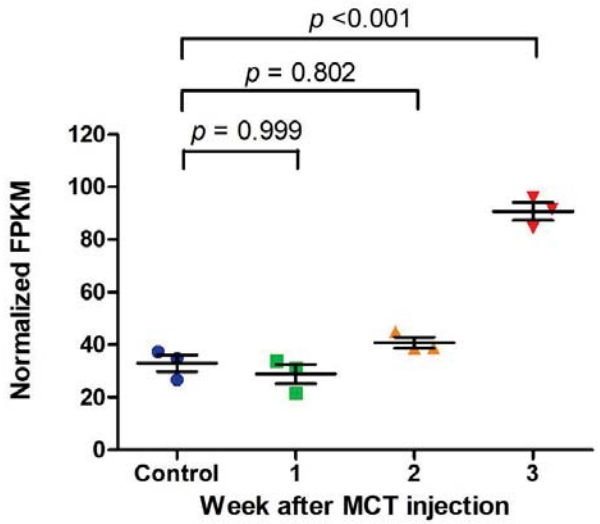

Figure 2

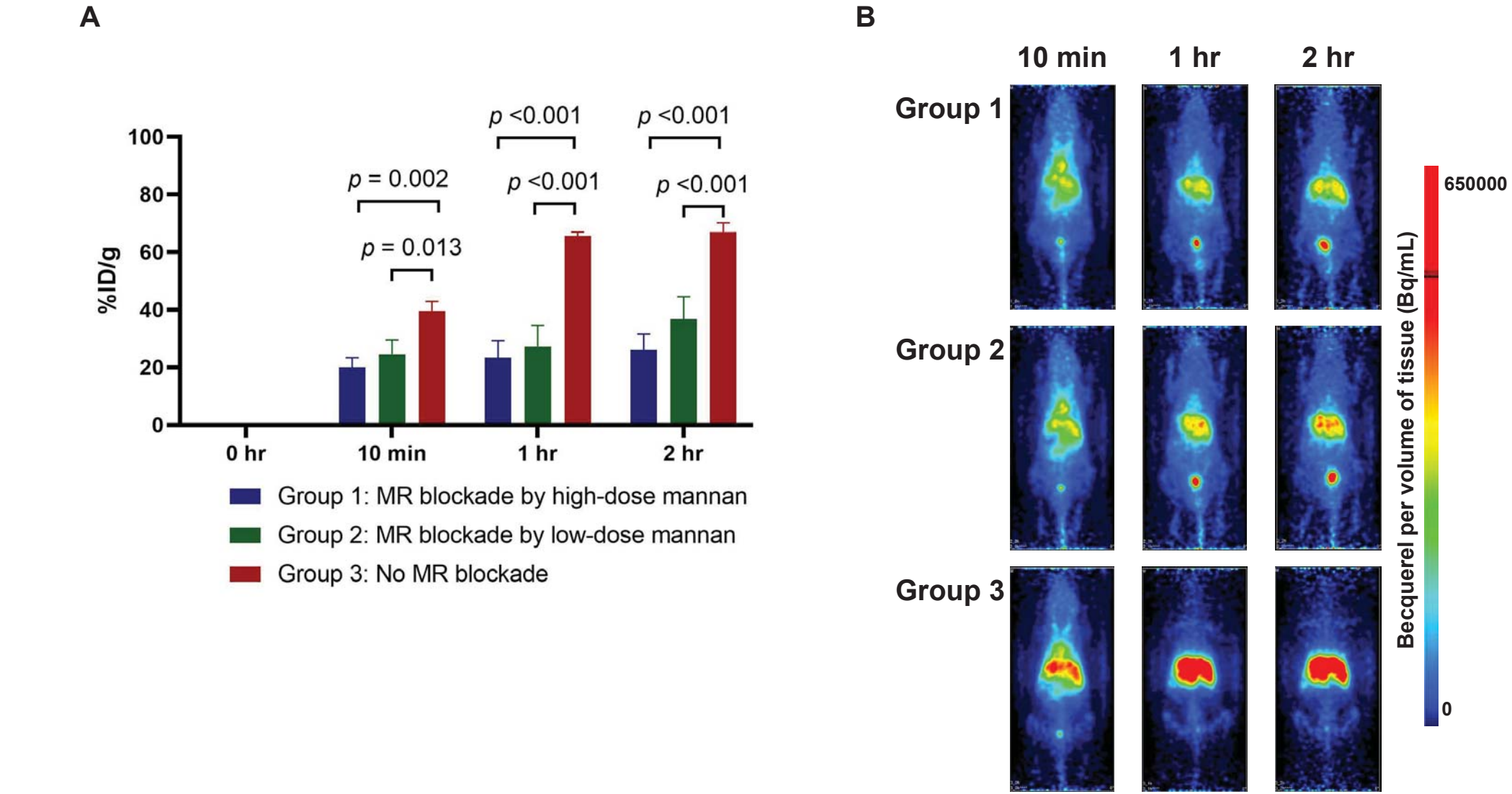

AJRCCM Articles in Press. Published on 19-July-2019 as 10.1164/rccm.201903-0639OC

Figure 3

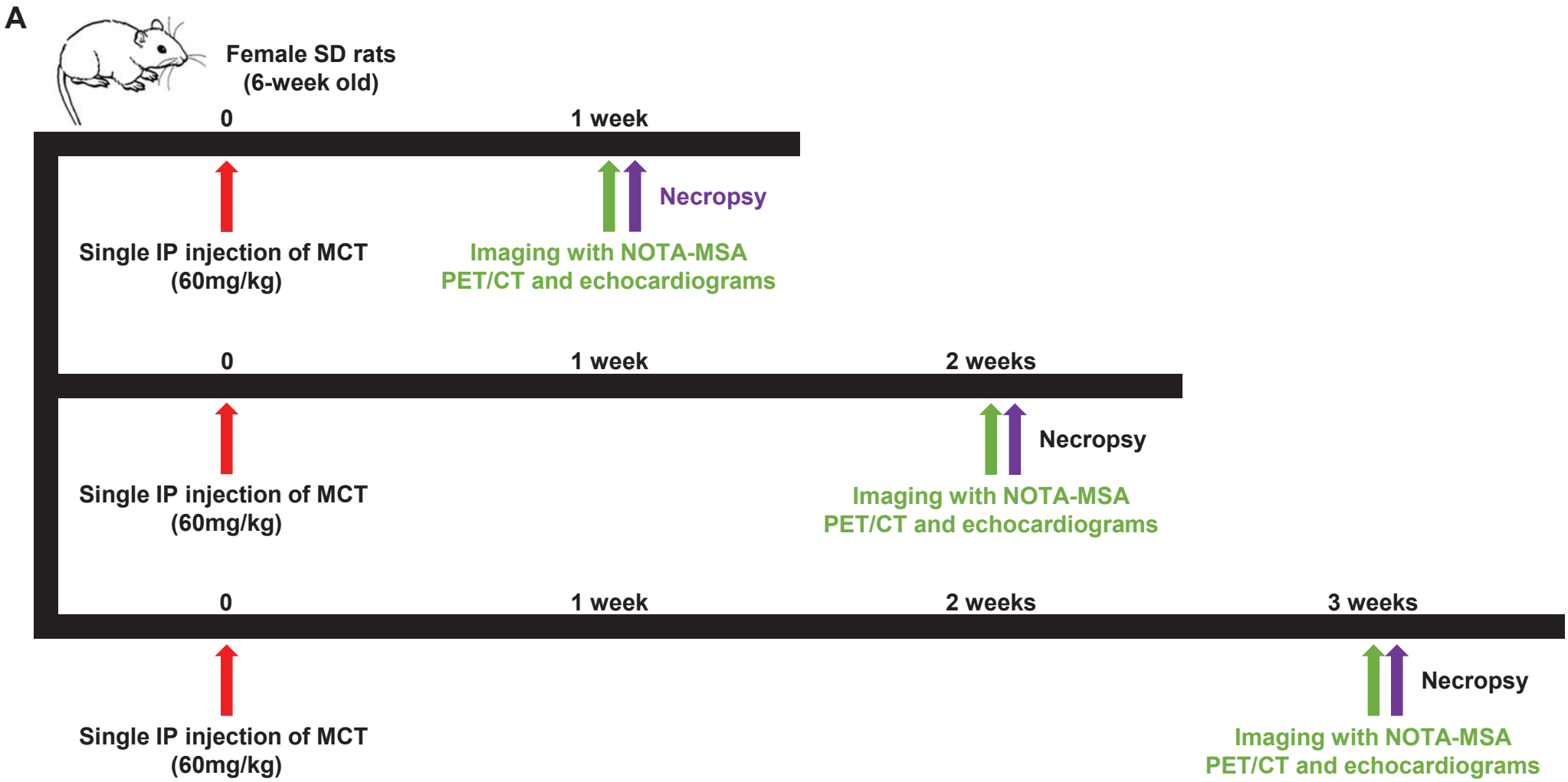

Figure 3

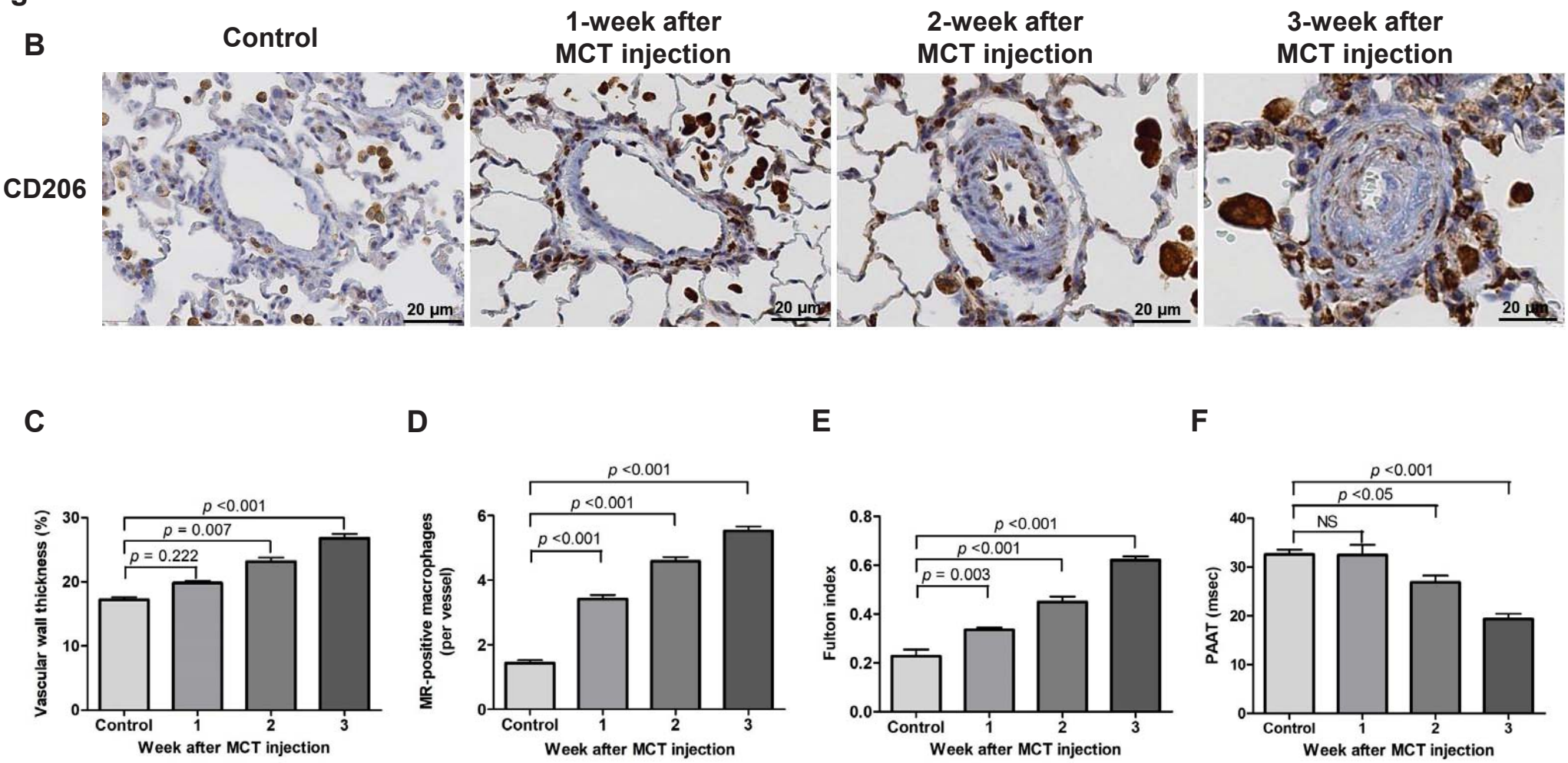

AJRCCM Articles in Press. Published on 19-July-2019 as 10.1164/rccm.201903-0639OC

Figure 3

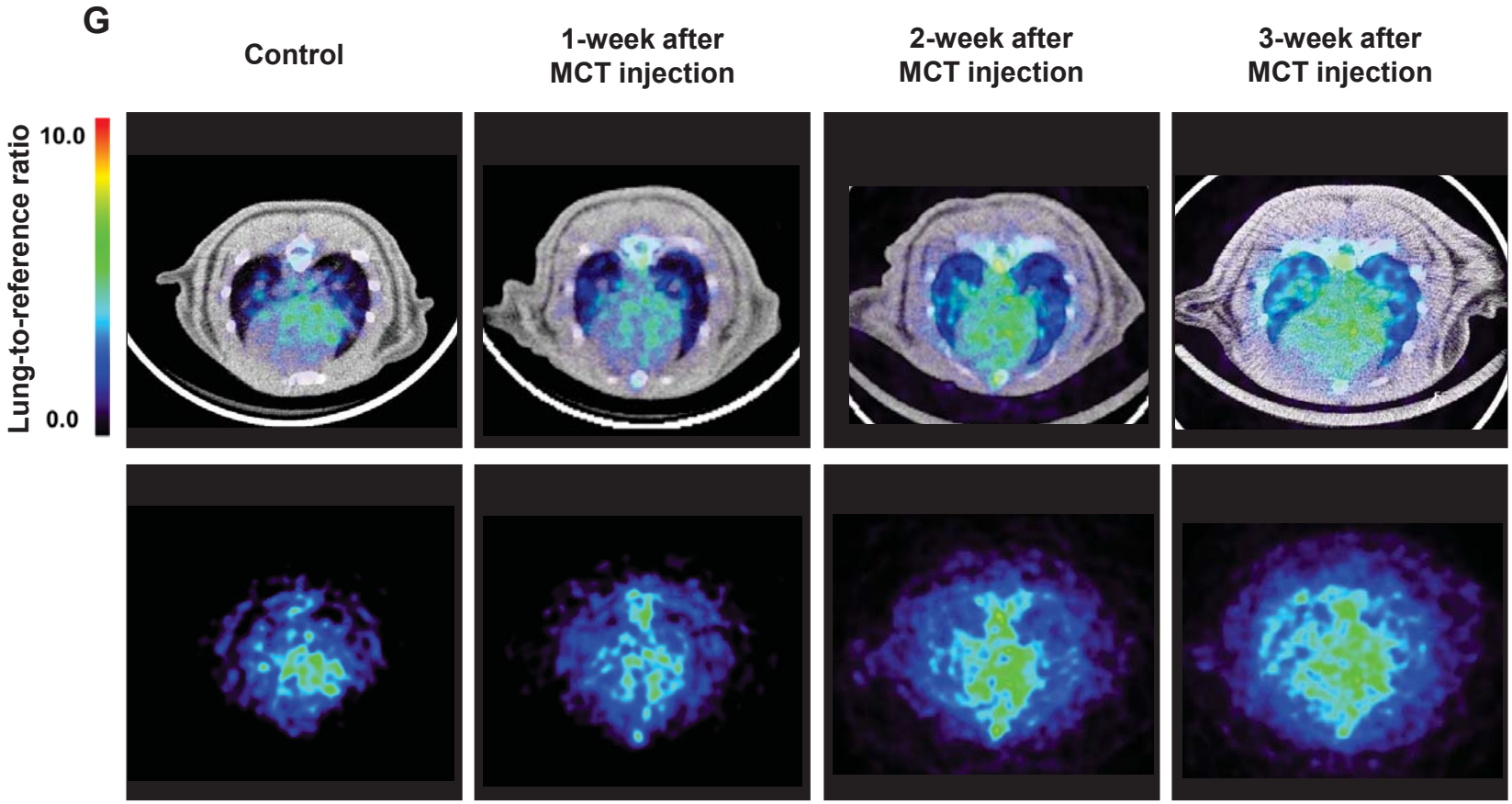

Figure 3

H

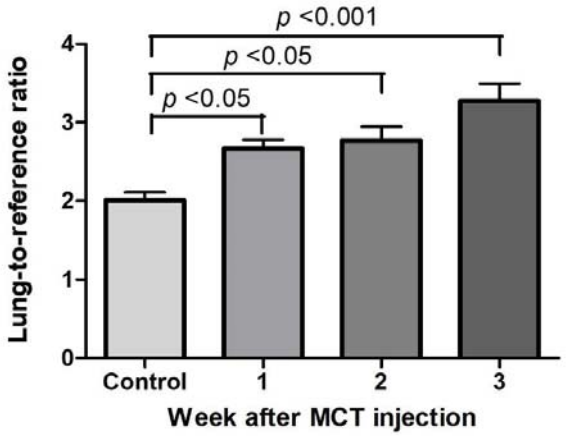

I

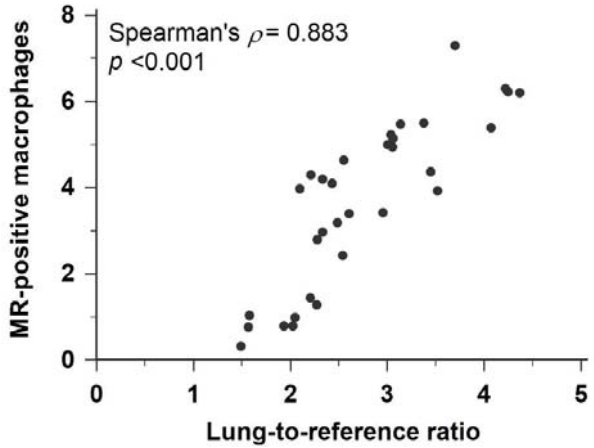

AJRCCM Articles in Press. Published on 19-July-2019 as 10.1164/rccm.201903-0639OC

Figure 4

Figure 4

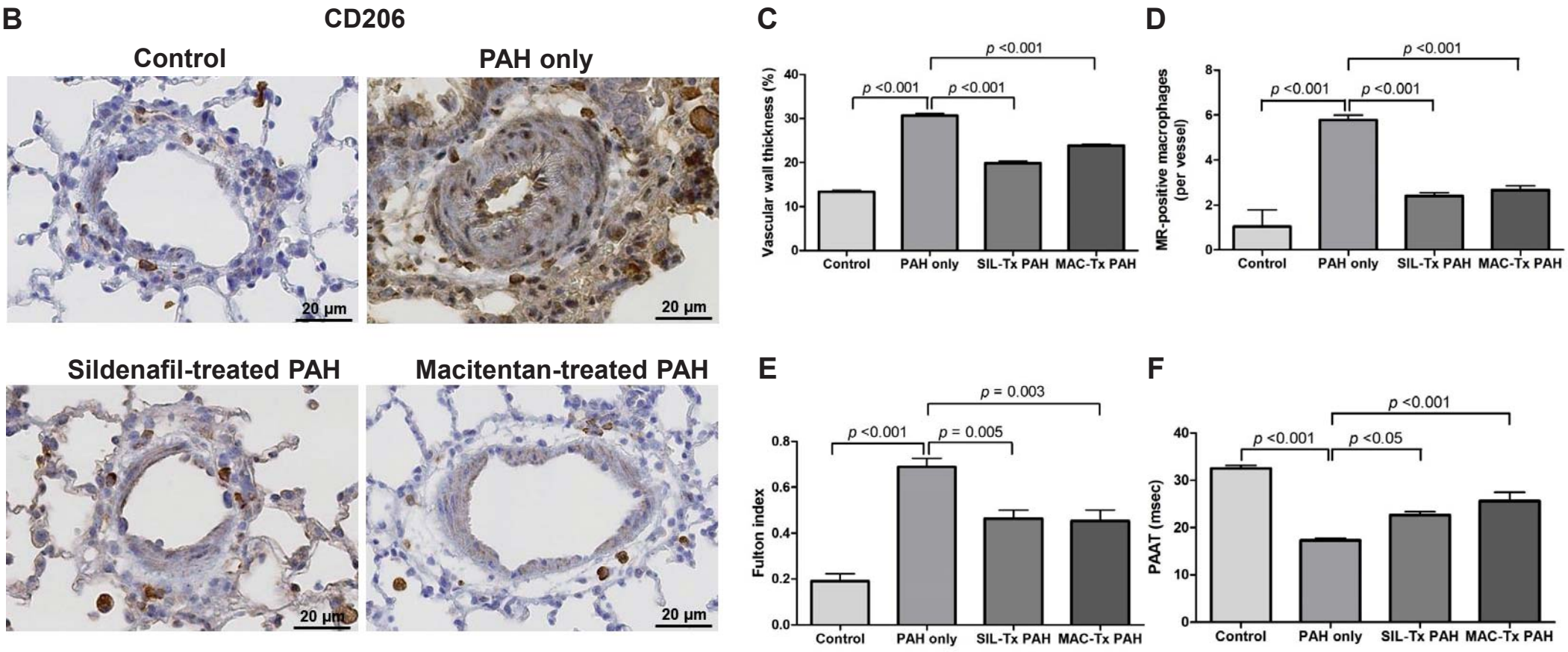

AJRCCM Articles in Press. Published on 19-July-2019 as 10.1164/rccm.201903-0639OC

Figure 4

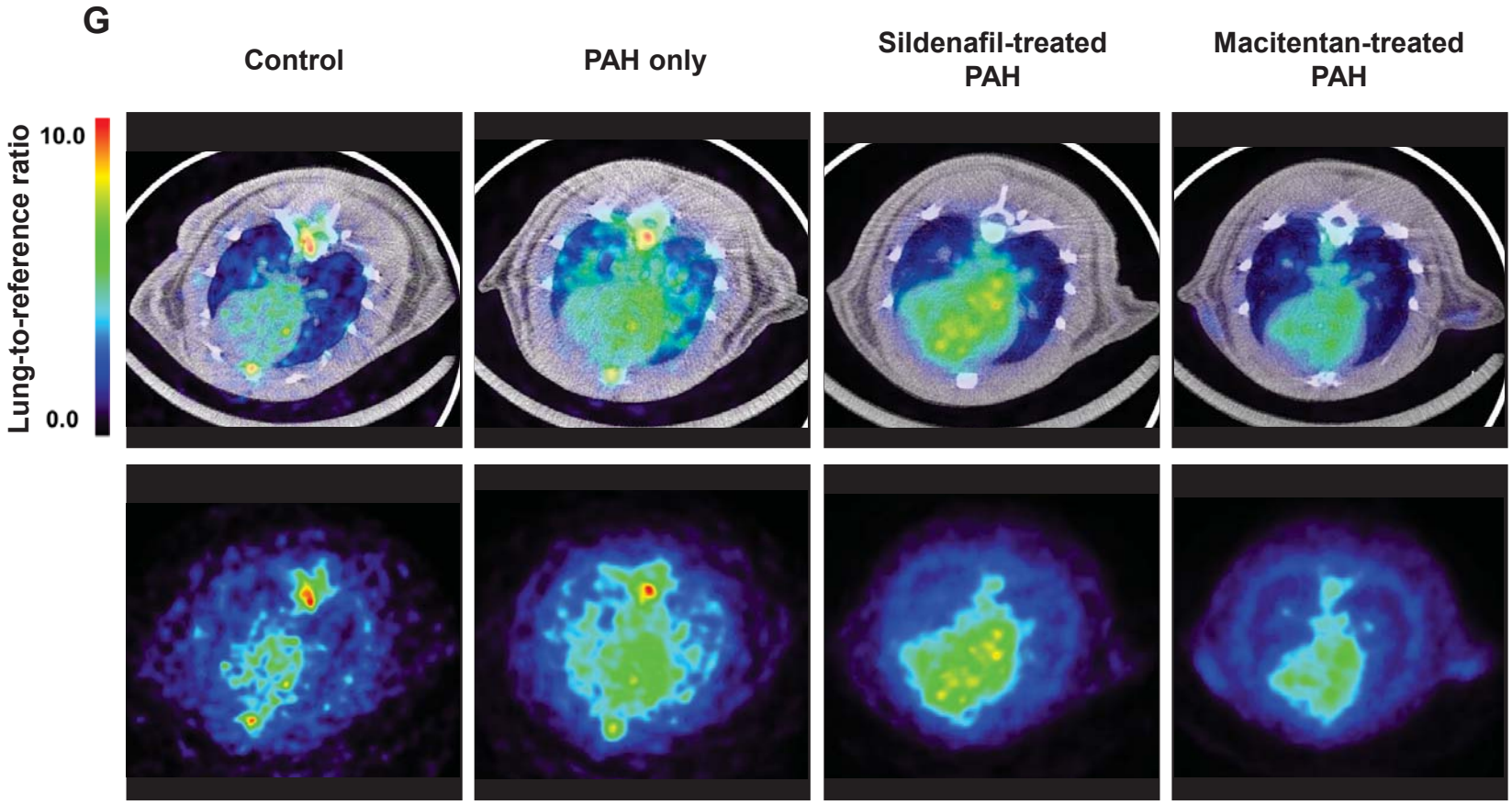

Figure 4

H

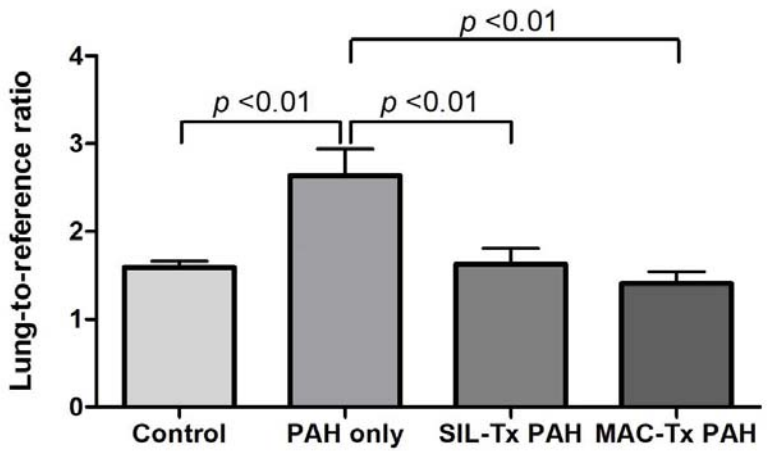

AJRCCM Articles in Press. Published on 19-July-2019 as 10.1164/rccm.201903-0639OC

Figure 5

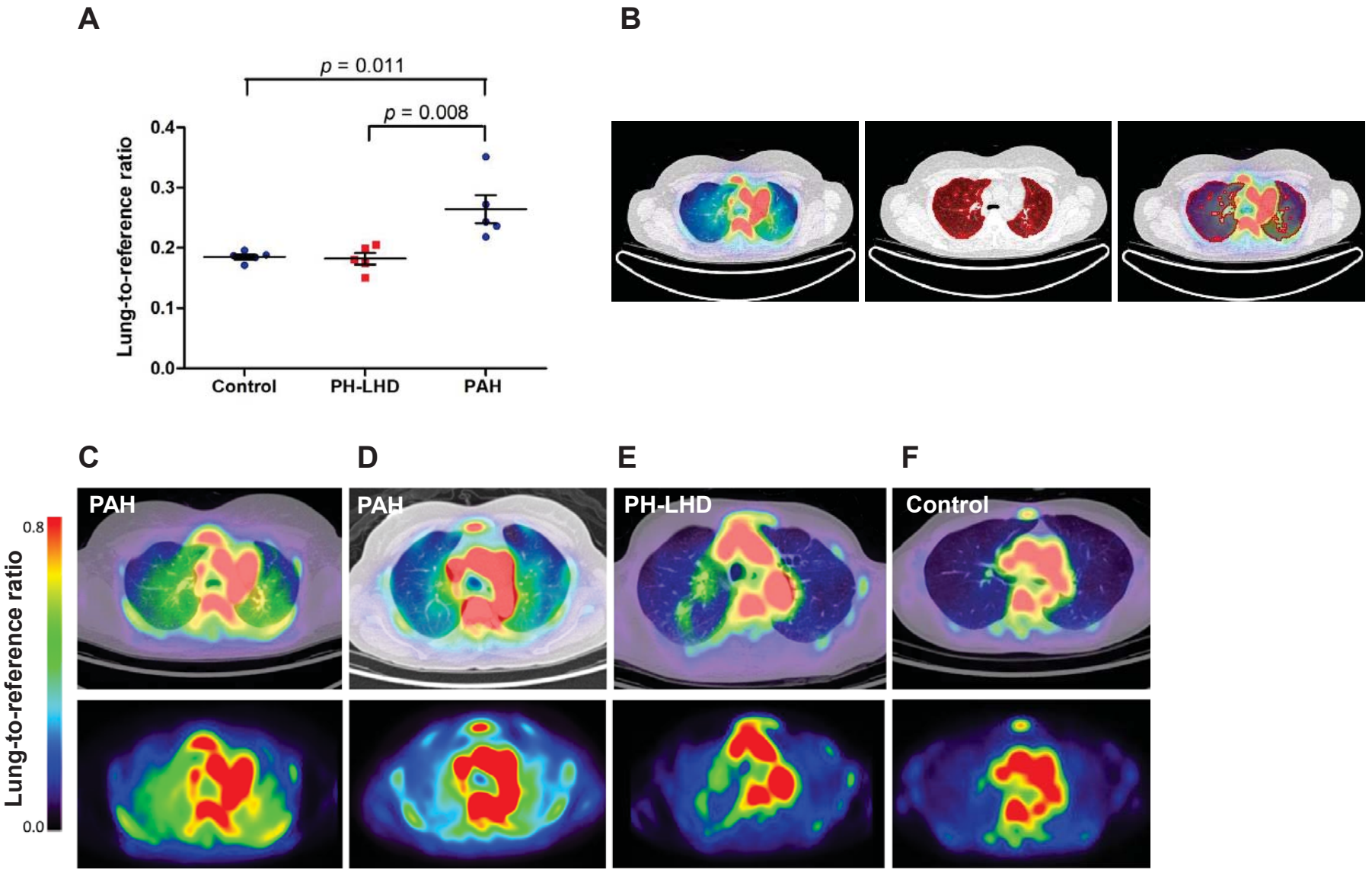

AJRCCM Articles in Press. Published on 19-July-2019 as 10.1164/rccm.201903-0639OC

Online Data Supplement

Assessment of Inflammation in Pulmonary Artery Hypertension by ^{68}Ga-Mannosylated Human Serum Albumin

Jun-Bean Park, Minseok Suh, Ji Yong Park, Jin Kyun Park, Yong-il Kim, Hyunah Kim, Ye Seul Cho, Hyejeong Kang, Kibyung Kim, Jae-Hoon Choi, Jin-Wu Nam, Hyung-Kwan Kim, Yun-Sang Lee, Jae Min Jeong, Yong-Jin Kim, Jin Chul Paeng, and Seung-Pyo Lee

SUPPLEMENTAL METHODS

Ethics statements of animal studies

All animal experimental protocol was approved by the Institutional Animal Care and Use Committee (IACUC) of Seoul National University Hospital (IACUC No. 14-0215-C1A0). The experiments also comply with the Guide for the Care and Use of Laboratory Animals (National Research Council, revised in 2011). Animal studies using radioactive tracers were approved by the local Institutional Biosafety Committee.

Transcriptome sequencing and data analysis

We examined the whole transcriptomic profile of the rat lung tissues collected after 1, 2, 3 weeks of subcutaneous monocrotaline administration and compared them with controls (n=3 per group). For these molecular analyses, the lung tissues were placed in RNAlater (Life Technologies, Carlsbad, CA, USA) according to the manufacturer's protocol and stored at −80 °C and the RNA quality checked, quantified, and sequenced as previously described (1). We focused on macrophage-related biological processes enriched with genes identified from

AJRCCM Articles in Press. Published on 19-July-2019 as 10.1164/rccm.201903-0639OC

t-test, using the annotations defined by the Gene Ontology (GO) Consortium. The enrichments of gene clusters in GO terms were assessed using a gene set enrichment test to compare the number of genes in each cluster associated with the studied meta-data to its expected value in the genome (12,750 genes).

Preparation of ^{68}Ga-NOTA-MSA

The 1,4,7-triazacyclononane-N,N,N-triacetic acid (NOTA) mannosylated human serum albumin (MSA) was synthesized as previously described (2). Briefly, 5.5mg α-D-mannopyranosylphenyl isothiocyanate (SCN-mannose) (Sigma-Aldrich, St. Louis, MO, USA) was conjugated with 20mg human serum albumin (Sigma-Aldrich) to synthesize MSA. This reaction was performed in 0.1M sodium carbonate buffer (pH 9.5) at room temperature for 20hrs. Thereafter, MSA was conjugated to 10mg SCN-NOTA, a bifunctional chelating agent, in 0.1M sodium carbonate buffer (pH 9.5) at room temperature for 1hr. The final product, ^{68}Ga-NOTA-MSA, was synthesized by labeling 1mg of NOTA-MSA (in 1ml of normal saline) with 1ml of $^{68}GaCl_3$ (in 0.1N HCl) (^{68}Ge/^{68}Ga generator from Eckert & Ziegler, Berlin, Germany).

Rat model of PAH

Pulmonary hypertension (PH) was induced in 6-week old female Sprague-Dawley rats by an intraperitoneal single injection of monocrotaline (60mg/kg, Sigma-Aldrich, St. Louis, MO, USA) with ^{68}Ga-NOTA-MSA PET/CT scans and echocardiograms weekly thereafter. Rats were euthanized at various time points (week 1, 2, and 3) after monocrotaline injection, and the lungs were harvested for pathological characterization ($n \geq 10$ per group).

Histologic analysis

Immunohistochemistry was performed as previously described (3). The degree of pulmonary arteriolar remodeling was determined by the ratio of medial wall thickness to the external diameter (i.e., percent wall thickness) of small muscular pulmonary arterioles (≤150μm outer diameter) on hematoxylin and eosin (H&E)-stained lung sections using ImageJ (40 vessels per animal, taken randomly throughout lung tissue) (n=8 per group). The primary antibodies used to characterize macrophages were mouse anti-rat ED1 (CD68) (1:500; Abcam, Cambridge, MA, USA) and rabbit anti-mouse MRC-1 (CD206) (1:8000; Abcam, Cambridge, MA, USA). We counted MR-positive macrophages near the pulmonary arterioles selected as described above (n=8 per group). The RV and left ventricular (LV) free wall and interventricular septum were harvested and weighed. The degree of RV hypertrophy was expressed as the Fulton index, the ratio of the RV free wall weight to LV free wall plus interventricular septum weight (n=8 per group).

To assess the role of ^{68}Ga-NOTA-MSA PET/CT in monitoring treatment response to PAH therapy, rats were treated with either oral macitentan (30mg/kg/day; Actelion Pharmaceuticals, Allschwil, Switzerland) or sildenafil (25mg/kg/day; Hanall Biopharma, Seoul, Republic of Korea), the representative endothelin receptor antagonist or phosphodiesterase type 5 inhibitor used in PAH patients, respectively, from the time of the initial monocrotaline injection. Imaging and pathological studies were performed 3 weeks after the initial monocrotaline injection (n≥5 per group for imaging experiments, n=5 per group for pathological analyses). After harvest of the lung tissue, we quantified percent wall thickness and the number of MR-positive macrophages in the lungs (40 vessels per animal, taken randomly throughout the whole lung tissue).

Hemodynamic assessment

Transthoracic echocardiography was performed as previously described (4), using an

AJRCCM Articles in Press. Published on 19-July-2019 as 10.1164/rccm.201903-0639OC

ultrasound machine (Nemio, Toshiba Medical System, Tokyo, Japan) equipped with a 9-MHz transducer. Spontaneously breathing rats were lightly anesthetized with the lowest dose of isoflurane inhalant as possible (initially 4% isoflurane mixed with oxygen, then maintained with 2~3% isoflurane during imaging). Pulsed-wave Doppler at the right ventricle outflow tract was used to measure pulmonary arterial acceleration time (PAAT) from the time of the onset of systolic flow to peak pulmonary outflow velocity and an average of 5 consecutive beats was obtained for analyses. All echocardiographic measurements were performed by an experienced sonographer with >5 years' experience in animal experiment, who was blinded to the group at the time of echocardiography.

Assessment of specificity of ^{68}Ga-NOTA-MSA tracer for MR

To validate the feasibility of ^{68}Ga-NOTA-MSA PET/CT assessment and its specificity to MR, biodistribution analysis of ^{68}Ga-NOTA-MSA was performed in 10-week old female BALB/c mice and also, in PAH rats. Mannan solution (25 mg/mL) was prepared as a MR blocker. Animals were divided into 3 groups (n=4 per group): group 1 (^{68}Ga-NOTA-MSA [24μCi] + MR blockade with high-dose mannan [2,500μg/animal]), group 2 (^{68}Ga-NOTA-MSA [24μCi] + MR blockade with low-dose mannan [500μg/animal]), and group 3 (^{68}Ga-NOTA-MSA [24μCi] + no MR blockade). The PET scans were obtained using a small-animal PET scanner (G4 PET X-RAY scanner; Sofie Biosciences, Culver City, CA, USA) with a scan time of 5 minutes at 10 minutes, 1 hour, and 2 hours after injection. The results were expressed as the percentage injected dose per gram of tissue (%ID/g).

^{68}Ga-NOTA-MSA PET/CT image acquisition and analysis

PET images were obtained by list mode in isoflurane-anaesthetized rats, for 60 minutes after intravenous administration of ^{68}Ga-NOTA-MSA (55.5MBq) using a small-animal PET/CT

scanner (eXplore VISTA, GE Healthcare, WI, USA). Based on a pilot analysis of dynamic images, static PET images were reconstructed using images acquired during 40–60 minutes post-injection (Supplemental Figure 1). Image reconstruction was conducted as described previously (5). Briefly, the scanned images were reconstructed by using a 3-dimensional ordered-subsets expectation maximization algorithm with random and scatter corrections. The voxel size was $0.3875\times0.3875\times0.775mm^3$. The degree of ^{68}Ga-NOTA-MSA uptake were measured by drawing regions of interest (ROI) at the lung and the reference tissue (back muscle) on the co-registered trans-axial PET/CT images, and the degree of ^{68}Ga-NOTA-MSA uptake in the lung was presented as the lung-to-reference ratio (LRR). The paraspinal muscle was selected as the reference tissue in this animal experiment, since in rats, superior vena cava was too small to serve as the reference.

Organ biodistribution assay of ^{68}Ga-NOTA-MSA in rat models of PAH

To validate the feasibility of PET/CT assessment, necropsy-based biodistribution analysis of ^{68}Ga-NOTA-MSA was performed at 3 weeks in the monocrotaline rat model of PAH, as well as in control animals. Animals were sacrificed 1 hour after injection of ^{68}Ga-NOTA-MSA (1.85MBq). The lung, muscle, and blood were collected and the radioactivity in each sample was measured using gamma-scintillation counter (Cobra II, Packard Instruments, Meriden, CT, USA). The results were expressed as %ID/g.

Human studies

Human studies were conducted in accordance with the latest Declaration of Helsinki and the study protocol was reviewed and approved by the Institutional Review Board (IRB) of Seoul National University Hospital (IRB No. 1506-156-686). All subjects gave written informed consent for study enrollment. From April 2014, we prospectively recruited 5 patients with

AJRCCM Articles in Press. Published on 19-July-2019 as 10.1164/rccm.201903-0639OC

idiopathic PAH or connective tissue disease-related PAH, who were confirmed by cardiac catheterization. The diagnosis of PAH was based on the standard definition of mean PAP≥25mmHg, pulmonary artery wedge pressure (PAWP)≤15mmHg, and pulmonary vascular resistance (PVR)>3 wood unit (6, 7). Five age-, sex-, and body mass index-matched healthy volunteers served as a normal control group. Five patients with PH due to left heart disease (PH-LHD) served as another control group. Major exclusion criteria were 1) the presence of concomitant significant lung disease, such as interstitial lung disease or chronic obstructive pulmonary disease, 2) the presence of pulmonary thromboembolism, and 3) the presence of hematologic disorders. For patients with PH-LHD as well as those with PAH, we also excluded patients who refused to undergo cardiac catheterization.

The PET/CT was performed using a dedicated scanner (Biograph 40, Siemens Healthcare, Knoxville, TN, USA) with 3-dimensional mode. After low-dose CT scan, ^{68}Ga-NOTA-MSA (185MBq) was injected into the antecubital vein, and PET image of the chest area was obtained for 60 minutes. The PET images were reconstructed using images acquired 30–60 minutes post-injection. Images were reconstructed on 256×256 matrices using an iterative algorithm (ordered-subset expectation maximization; 4 iterations and 8 subsets). The ^{68}Ga-NOTA-MSA PET/CT images were batch-analyzed by an investigator blinded to the clinical and hemodynamic data of the study participants. The ROIs were drawn for lungs and the reference tissue (superior vena cava) (8), and the degree of uptake in the lungs were expressed as the LRR.

Statistical analysis

Continuous and categorical data were presented as median (range) and number (percent), respectively. The Student t test or Mann-Whitney U test was used to compare continuous variables, and the chi-square test or Fisher's exact test was used to compare categorical

variables as appropriate. One-way analysis of variance (ANOVA) followed by Bonferroni post-hoc test was performed for comparisons between multiple groups. In cases where the data was not normally distributed, Kruskal-Wallis test followed by Dunn's multiple comparison test was used to compare the mean ranks. Spearman's ρ was used to quantify the correlations between variables. Statistical analysis was performed with SPSS version 23.0 (SPSS Inc., Chicago, IL, USA). A two-sided p value <0.05 was considered significant.

AJRCCM Articles in Press. Published on 19-July-2019 as 10.1164/rccm.201903-0639OC

References

1. Baek A, Cho SR, Kim SH. Elucidation of Gene Expression Patterns in the Brain after Spinal Cord Injury. *Cell Transplant* 2017; 26: 1286-1300.

2. Choi JY, Jeong JM, Yoo BC, Kim K, Kim Y, Yang BY, Lee YS, Lee DS, Chung JK, Lee MC. Development of 68Ga-labeled mannosylated human serum albumin (MSA) as a lymph node imaging agent for positron emission tomography. *Nuclear medicine and biology* 2011; 38: 371-379.

3. Park JB, Kim BK, Kwon YW, Muller DN, Lee HC, Youn SW, Choi YE, Lee SW, Yang HM, Cho HJ, Park KW, Kim HS. Peroxisome proliferator-activated receptor-gamma agonists suppress tissue factor overexpression in rat balloon injury model with paclitaxel infusion. *PLoS One* 2011; 6: e28327.

4. Kim KH, Kim HK, Chan SY, Kim YJ, Sohn DW. Hemodynamic and Histopathologic Benefits of Early Treatment with Macitentan in a Rat Model of Pulmonary Arterial Hypertension. *Korean Circ J* 2018; 48: 839-853.

5. Lee SP, Im HJ, Kang S, Chung SJ, Cho YS, Kang H, Park HS, Hwang DW, Park JB, Paeng JC, Cheon GJ, Lee YS, Jeong JM, Kim YJ. Noninvasive Imaging of Myocardial Inflammation in Myocarditis using 68Ga-tagged Mannosylated Human Serum Albumin Positron Emission Tomography. *Theranostics* 2017; 7: 413-424.

6. Simonneau G, Gatzoulis MA, Adatia I, Celermajer D, Denton C, Ghofrani A, Gomez Sanchez MA, Krishna Kumar R, Landzberg M, Machado RF, Olschewski H, Robbins IM, Souza R. Updated clinical classification of pulmonary hypertension. *J Am Coll Cardiol* 2013; 62: D34-41.

7. McLaughlin VV, Shah SJ, Souza R, Humbert M. Management of pulmonary arterial hypertension. *J Am Coll Cardiol* 2015; 65: 1976-1997.

8. Rudd JH, Myers KS, Bansilal S, Machac J, Rafique A, Farkouh M, Fuster V, Fayad ZA.

(18)Fluorodeoxyglucose positron emission tomography imaging of atherosclerotic plaque inflammation is highly reproducible: implications for atherosclerosis therapy trials. *J Am Coll Cardiol* 2007; 50: 892-896.

AJRCCM Articles in Press. Published on 19-July-2019 as 10.1164/rccm.201903-0639OC

SUPPLEMENTAL FIGURE LEGENDS

Figure E1. Time-activity curve of representative cases

(A-C) Time-activity curve of the PET tracer in rats. **(A)** A case with high lung-to-reference ratio (LRR) shows slower decrease of LRR compared with a case with low LRR in rat studies where muscle was used as the reference tissue. After 40 minutes post-injection, the curves show patterns of plateau in both cases and LRR was measured on static images of 40–60 minutes post-injection. Time-activity curves of each region-of-interest in cases with high LRR and low LRR are shown in **(B)** and **(C)**, respectively. **(D-F)** Time-activity curve of the PET tracer in humans **(D)**. In human studies where blood pool was used as the reference tissue, LRR rapidly increased at an early phase and gradually plateaued with time, both in a case with high LRR and another case with low LRR. Time-activity curves of each region-of-interest in cases with high LRR and low LRR are shown in **(E)** and **(F)**, respectively. LRR= lung-to-reference ratio; SVC=superior vena cava

Figure E2. Representative images of ROI drawn for analysis

Red colored area in the bottom panel indicates regions of interest (ROI) used to assess lung uptake of ^{68}Ga-NOTA-MSA on PET images. The color scale bar indicates the lung-to-reference ratio.

Figure E3. Histological and echocardiographic changes of the lung in PAH progression

(A) Note the thickened pulmonary arteriolar wall at 2 and 3 weeks after monocrotaline injection and prominent infiltration of ED1-positive macrophages around the pulmonary arteriole at 1, 2, and 3 weeks after monocrotaline administration. **(B)** Representative images of Doppler echocardiography-derived pulmonary artery acceleration time (PAAT) which decreased with the progression of PAH. MCT=monocrotaline.

Figure E4. Histological changes of the lung after treatment with PAH-targeted therapy

Histological changes after 3-week oral administration of sildenafil (25mg/kg/day) or macitentan (30mg/kg/day) from the time of monocrotaline injection. Compared with the PAH rat without treatment (panels in the second column), note the attenuation of monocrotaline-induced pulmonary arteriole muscularization of the PAH rat treated with sildenafil or macitentan (panels in the third and fourth columns, respectively). PAH=pulmonary artery hypertension.

Figure E5. Evaluation of PAH based on pathophysiologic aspects

Schematic representation of the pathological processes of PAH and corresponding evaluation tools.

Left panel: Conventional diagnostic modalities include right heart catheterization and echocardiography, which can assess hemodynamic abnormalities in PAH in an invasive or noninvasive manner. **Right panel:** ^{68}Ga-NOTA-MSA PET/CT imaging can be used as a marker of the underlying pathological processes of PAH (i.e., infiltration of macrophages in pulmonary vasculature) and thus may provide useful diagnostic clues to distinguish PAH from PH-LHD as well as normal subjects.

PAP=pulmonary artery pressure; PVR=pulmonary vascular resistance; RV=right ventricular.

AJRCCM Articles in Press. Published on 19-July-2019 as 10.1164/rccm.201903-0639OC

SUPPLEMENTAL TABLES

Table E1. Inclusion and Exclusion Criteria for the Human Study

Inclusion criteria	Exclusion criteria
Mean PAP≥25mmHg,	The presence of significant lung disease, such as ILD or COPD
Pulmonary artery wedge pressure (PAWP) ≤15mmHg	The presence of pulmonary thromboembolism
Pulmonary vascular resistance (PVR) >3 wood unit	The presence of hematologic disorders

COPD, chronic obstructive pulmonary disease; ILD, interstitial lung disease; PAP, pulmonary artery pressure; PAWP, pulmonary artery wedge pressure; PVR, pulmonary vascular resistance

Table E2. Correlation between ^{68}Ga-NOTA-MSA uptake and PAH parameters

	Spearman's ρ	*p*
Degree of lung infiltration of MR-positive macrophages (per vessel)	0.909	<0.001
Vascular wall thickness (%)	0.505	0.003
Pulmonary artery acceleration time (msec)	-0.468	0.002
Fulton's index	0.717	<0.001

MR, mannose receptor

AJRCCM Articles in Press. Published on 19-July-2019 as 10.1164/rccm.201903-0639OC

Table E3. Organ Biodistribution Analysis of ^{68}Ga-NOTA-MSA in Post-Mortem Rats

Organ	Normal (n=6, %ID/g)	PAH (n=6, %ID/g)	*p*
Lung	0.12 ± 0.01 [0.12 (0.11 - 0.13)]	0.53 ± 0.13 [0.54 (0.42 – 0.62)]	<0.001
Muscle	0.01 ± 0.01 [0.01 (0.01 – 0.01)]	0.01 ± 0.01 [0.01 (0.01 – 0.02)]	0.151
Blood	0.11 ± 0.02 [0.10 (0.09 – 0.12)]	0.13 ± 0.02 [0.12 (0.11 – 0.14)]	0.118

Values given as number (percentage), mean±standard deviation, or median (interquartile range).

%ID/g denotes the mean percent injected dose per gram.

Table E4. Baseline Clinical Data of Each Study Participant

Subject No.	Group	Age, years	Sex	Height, cm	Weight, kg	PAH targeted therapy before the enrollment	CTD	ILD
1	Control	36	M	182	87	No	No	No
2	Control	45	F	160	49	No	No	No
3	Control	46	F	165	52	No	No	No
4	Control	54	F	150	48	No	No	No
5	Control	39	F	160	45	No	No	No
6	PH-LHD	70	F	156	45	No	SSc	Mild CTD-related ILD
7	PH-LHD	58	M	173	67	No	SSc	Mild CTD-related ILD, Mild localized BE
8	PH-LHD	71	F	150	52	No	No	No
9	PH-LHD	47	F	174	55	No	No	No
10	PH-LHD	56	M	166	53	No	No	No
11	PAH	58	F	153	46	Ambrisentan + Sildenafil	No	No
12	PAH	45	F	155	46	Bosentan + Iloprost	No	No

AJRCCM Articles in Press. Published on 19-July-2019 as 10.1164/rccm.201903-0639OC

13	PAH	36	F	168	72	Bosentan	No	No
14	PAH	23	F	157	62	No	No	No
15	PAH	23	M	170	67	Ambrisentan + Tadalafil	No	No

BE, bronchiectasis; CTD, connective tissue disease; ILD, interstitial lung disease, PAH, pulmonary artery hypertension; PH-LHD, pulmonary hypertension due to left heart disease; SSc, systemic sclerosis.

Table E5. Baseline Hemodynamic and ^{68}Ga-MSA-NOTA PET/CT Data of Each Study Participant

Subject No.	Group	Cardiac catheterization				^{68}Ga-NOTA-MSA PET/CT			
		Date of test	MPAP, mmHg	PAWP, mmHg	PVR, WU	Date of test	Lung, SUV	SVC, SUV	Lung-to-SVC SUV ratio
1	Control	N/A	N/A	N/A	N/A	2016-03-28	1393.1	8150.7	0.171
2	Control	N/A	N/A	N/A	N/A	2017-07-07	1504.2	8008.1	0.188
3	Control	N/A	N/A	N/A	N/A	2017-08-03	2110.0	10764.8	0.196
4	Control	N/A	N/A	N/A	N/A	2018-02-12	2599.2	14160.0	0.184
5	Control	N/A	N/A	N/A	N/A	2017-08-25	1878.7	10051.4	0.187
6	PH-LHD	2015-11-12	58	45	6.56	2015-11-24	2792.6	16005.0	0.174
7	PH-LHD	2016-02-11	33	26	1.35	2016-01-15	1820.4	9130.8	0.199
8	PH-LHD	2017-12-07	46	16	9.7	2017-12-04	2312.6	12801.0	0.181
9	PH-LHD	2017-09-01	40	18	7.9	2015-11-30	2301.2	11207.6	0.205
10	PH-LHD	2018-08-09	44	18	4.3	2018-08-20	3184.5	21046.0	0.151
11	PAH	2015-11-05	35	5	12.5	2017-05-26	2145.7	9859.0	0.218
12	PAH	2015-12-31	54	14	18.18	2015-11-18	2367.3	8690.8	0.272

AJRCCM Articles in Press. Published on 19-July-2019 as 10.1164/rccm.201903-0639OC

13	PAH	2017-11-28	65	13	16.56	2016-02-15	2367.9	10020.3	0.236
14	PAH	2017-12-07	32	14	5.08	2017-12-11	2679.7	7627.1	0.351
15	PAH	2017-09-01	62	12	18.7	2018-03-07	2043.9	8409.7	0.243

MPAP, mean pulmonary artery pressure; MSA, human serum albumin; N/A, not applicable; NOTA, 2-(*p*-isothiocyanatobenzyl)-1,4,7-triazacyclononane-1,4,7-triacetic acid; PAH, pulmonary artery hypertension; PAWP, pulmonary artery wedge pressure; PET/CT, positron emission tomography/computed tomography; PH-LHD, pulmonary hypertension due to left heart disease; PVR, pulmonary vascular resistance; SUV, standardized uptake value; SVC, superior vena cava.

Figure E1

AJRCCM Articles in Press. Published on 19-July-2019 as 10.1164/rccm.201903-0639OC

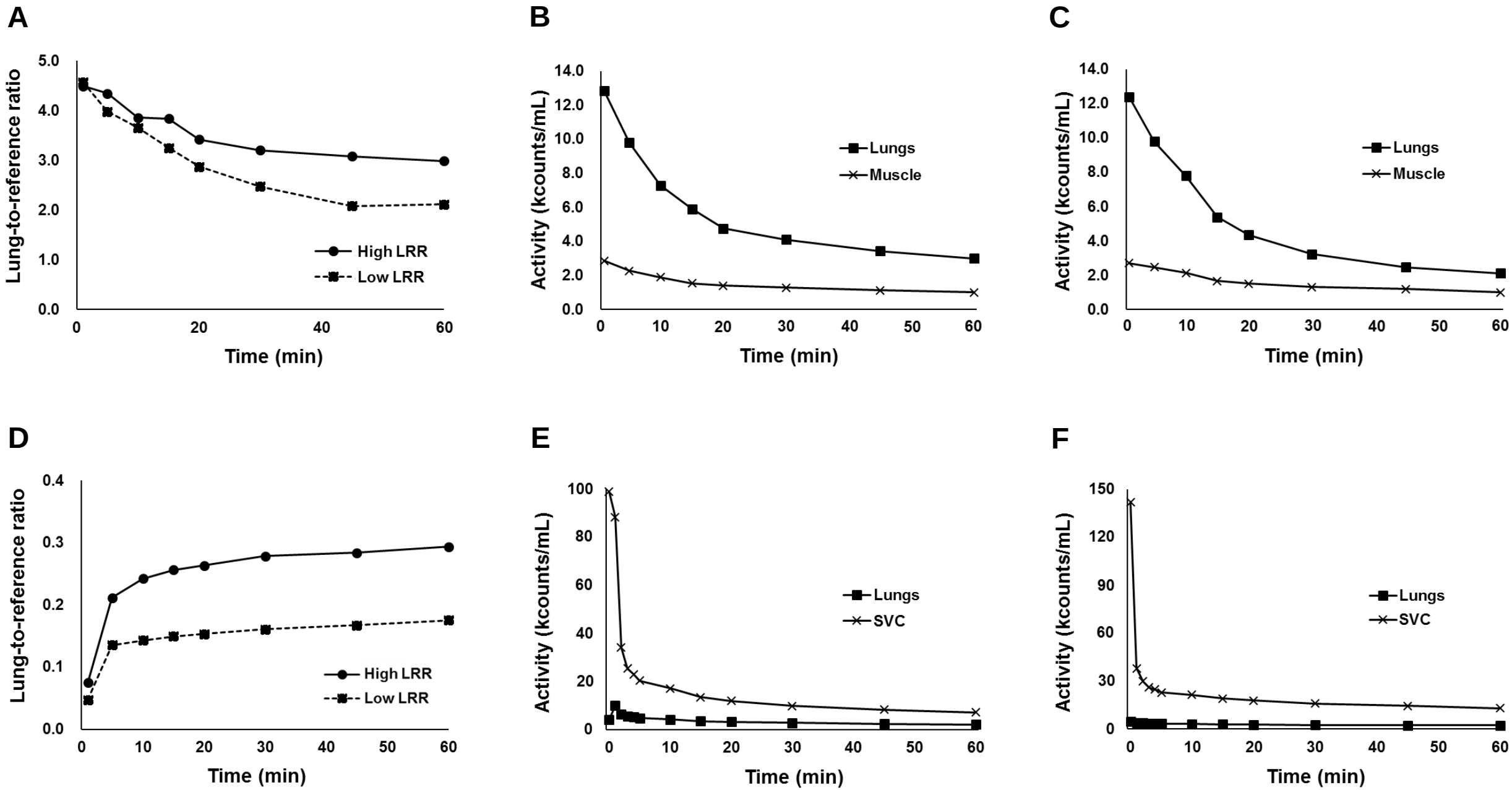

AJRCCM Articles in Press. Published on 19-July-2019 as 10.1164/rccm.201903-0639OC

Figure E2

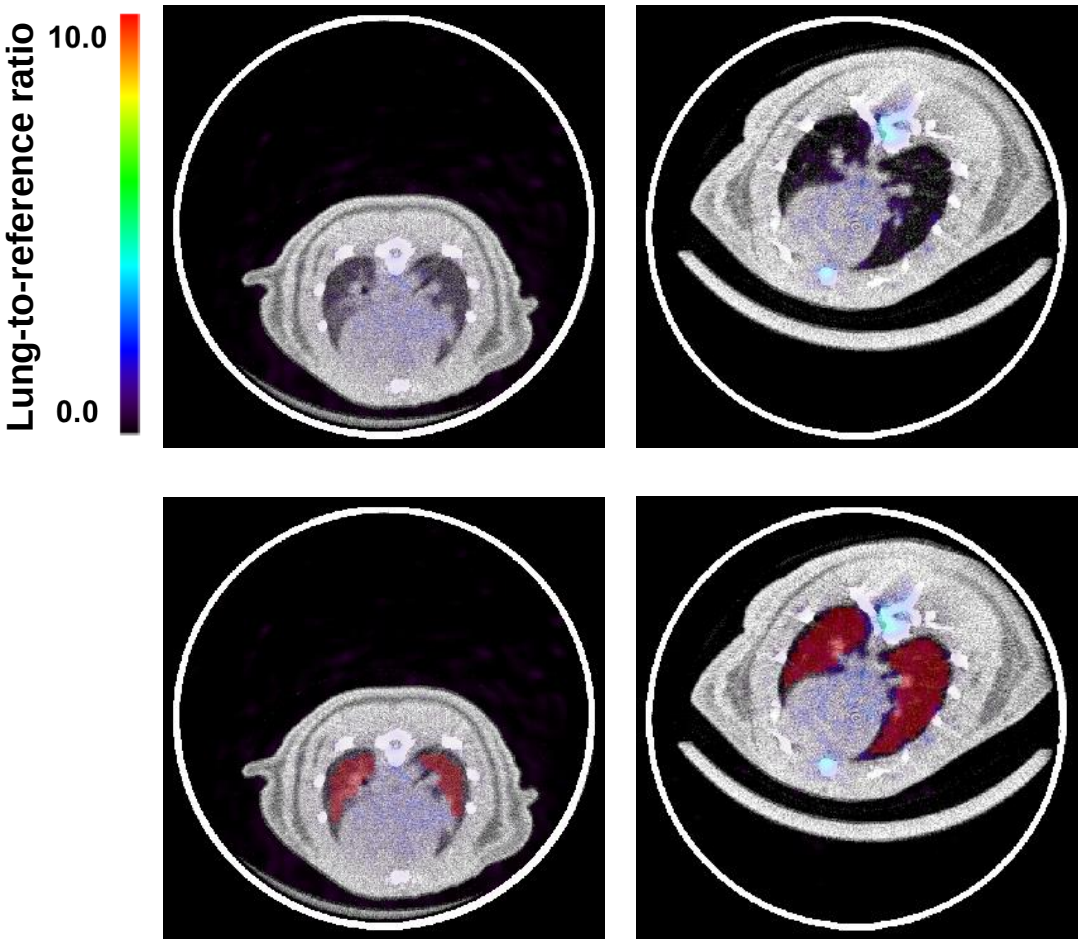

AJRCCM Articles in Press. Published on 19-July-2019 as 10.1164/rccm.201903-0639OC

A

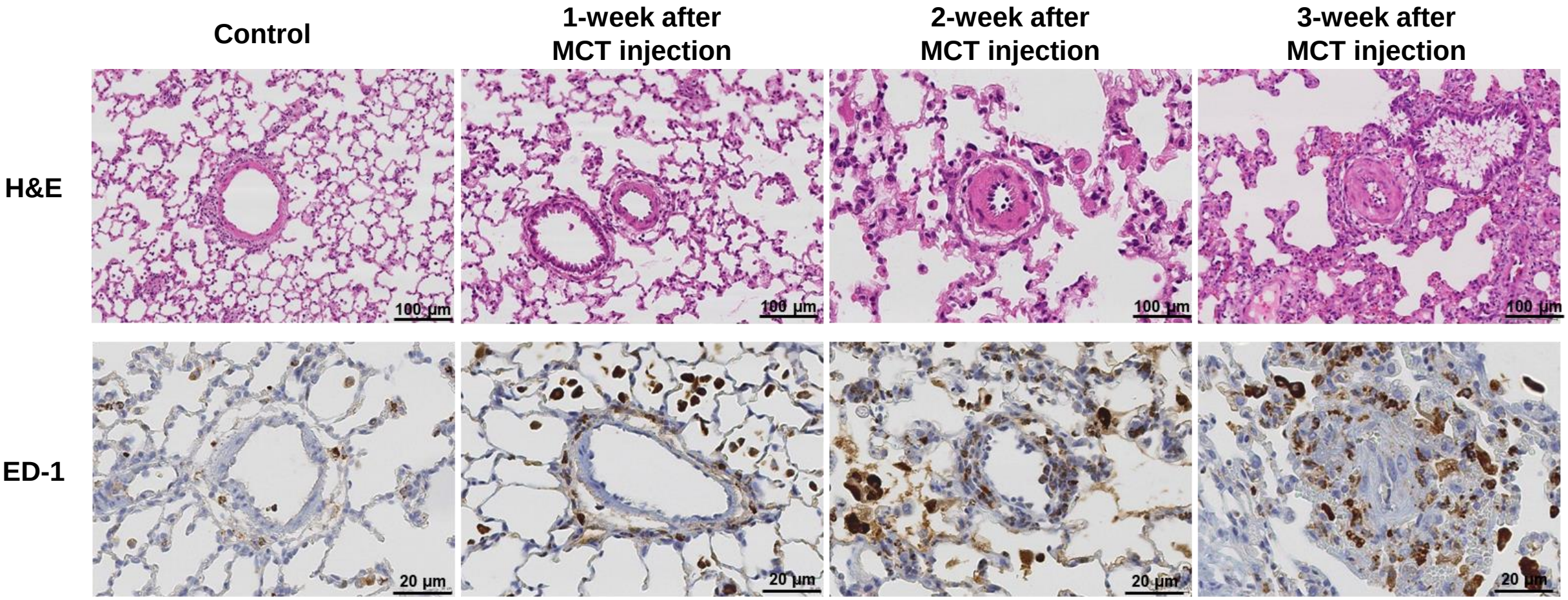

AJRCCM Articles in Press. Published on 19-July-2019 as 10.1164/rccm.201903-0639OC

Figure E3

B

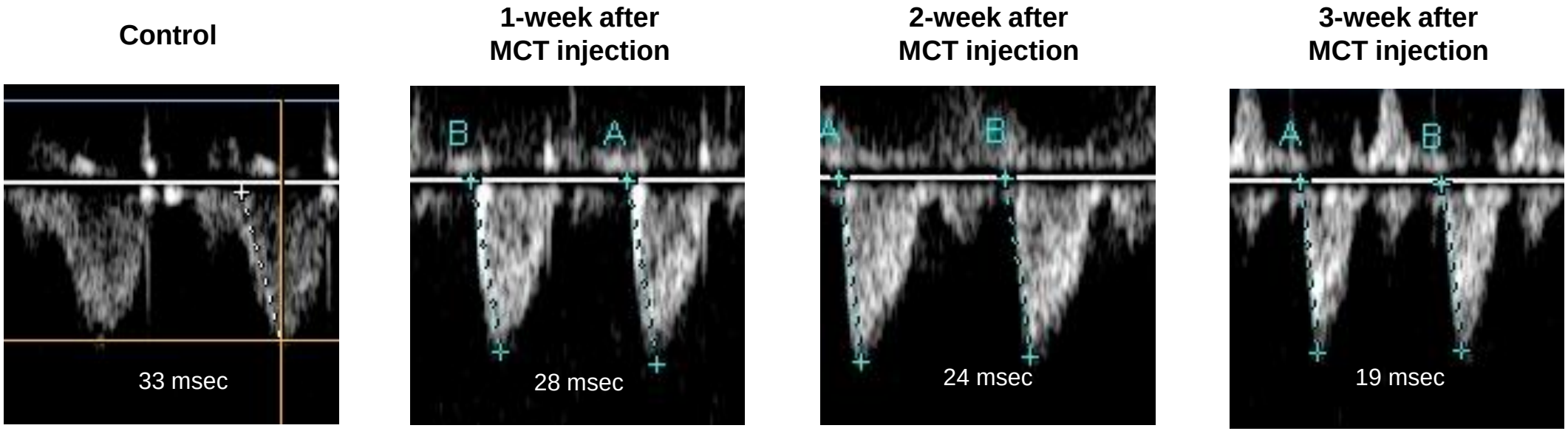

Figure E4

AJRCCM Articles in Press. Published on 19-July-2019 as 10.1164/rccm.201903-0639OC

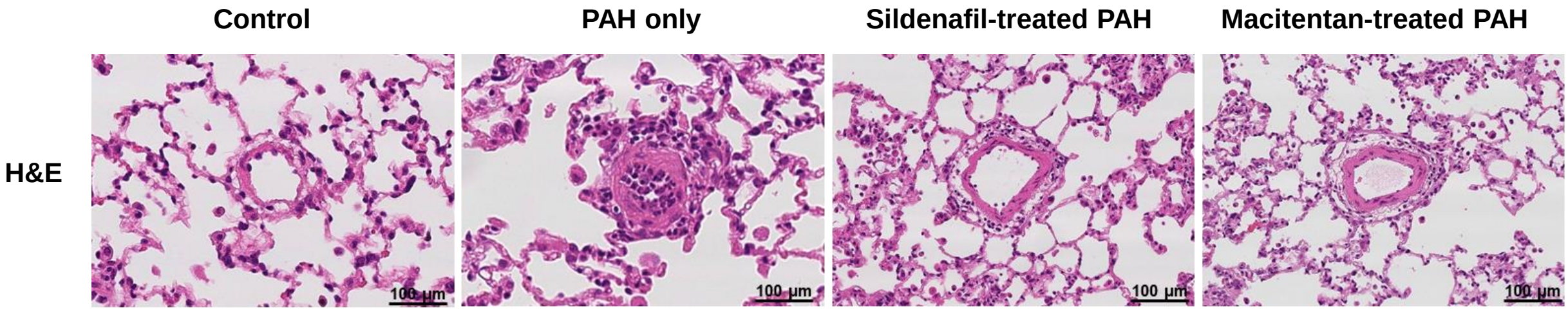

Figure E5

AJRCCM Articles in Press. Published on 19-July-2019 as 10.1164/rccm.201903-0639OC

Diagnosis of pulmonary artery hypertension based on pathophysiology

Hemodynamic deterioration

PAP↑, PVR ↑, RV dilatation & dysfunction

Invasive tool	Noninvasive tool
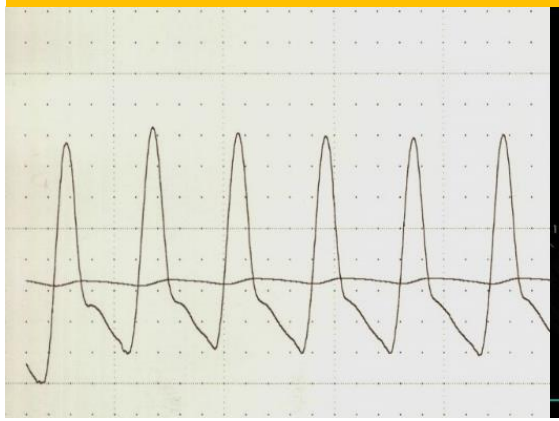	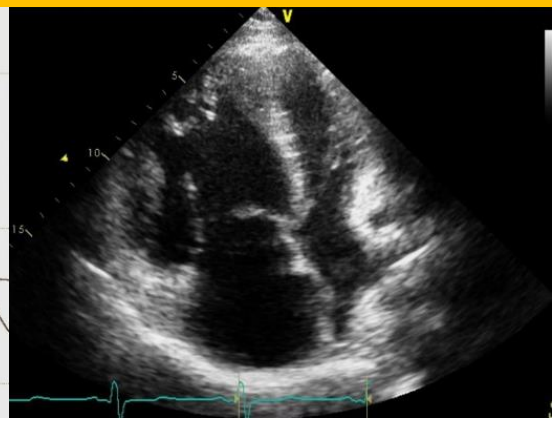

Inflammation / altered immune response

Macrophage activation & migration

Invasive tool	Noninvasive tool